Sustainable Materials and Technologies 35 (2023) e00581

Contents lists available at ScienceDirect

Sustainable Materials and Technologies

journal homepage: www.elsevier.com/locate/susmat

Poly(caprolactone)/lignin-based 3D-printed dressings loaded with a novel combination of bioactive agents for wound-healing applications

Juan Domínguez-Robles [a,b,*], Elias Cuartas-Gómez [c], Sean Dynes [a], Emilia Utomo [a], Qonita Kurnia Anjani [a,d], Usanee Detamornrat [a], Ryan F. Donnelly [a], Natalia Moreno-Castellanos [c,*], Eneko Larrañeta [a,*]

[a] School of Pharmacy, Queen's University Belfast, Lisburn Road 97, Belfast BT9 7BL, UK
[b] Department of Pharmacy and Pharmaceutical Technology, University of Seville, 41012 Seville, Spain
[c] CICTA, Department of Basic Sciences, Medicine School, Health Faculty, Universidad Industrial de Santander, Cra 27 calle 9, Bucaramanga 680002, Colombia
[d] Fakultas Farmasi, Universitas Megarezky, Jl. Antang Raya No. 43, Makassar 90234, Indonesia

ARTICLE INFO

Keywords:
Bioactive materials
3D printing
Antimicrobial dressings
Sustained release
Curcumin
D-Panthenol

ABSTRACT

Curcumin (CUR) has been shown to possess significant anti-inflammatory properties and significant wound healing potential. Additionally, lignin (LIG) is a renewable biomacromolecule with well-known antioxidant and antimicrobial properties, which makes this biomacromolecule a good candidate to be included in medical materials, such as wound dressings. Although many of the wound dressings used at present have interesting features, some are limited in terms of antibacterial properties. To address these limitations, in the present work, both CUR and LIG were combined with poly(caprolactone) (PCL), a biocompatible polymer, to obtain dressings with antioxidant and antimicrobial properties for wound healing treatment. Moreover, D-Panthenol (DPA) was included in the composite materials formulation due to its skin regenerative ability by enhancing epidermal differentiation. Semi-solid extrusion (SSE) 3D printing was used to manufacture wound dressings without the use of any solvents. 3D-printed dressings provided a sustained DPA and CUR release for periods of up to 4 and 35 days, respectively. A DPPH (2,2-diphenyl-1-picrylhydrozyl) assay was performed confirming that the presence of LIG and CUR provided antioxidant properties to the 3D-printed dressings. Additionally, these 3D-printed materials showed a marked resistance to adherence of *Staphylococcus aureus* when compared to the PCL control 3D-printed samples, resulting in substantial reductions of up to 89.9% and 98.9% after incubation periods of 4 h and 24 h respectively. Although, all of the 3D-printed materials were able to provide a supportive environment for cellular attachment, viability and growth, the combination of both bioactive compounds CUR and DPA exhibited the most significant values for cell viability and proliferation. *In vivo* wound healing study performed in Wistar rats showed that dressings containing these novel two compounds CUR and DPA exhibited marked improvement at any stage of the treatment process. Finally, histological examination revealed that dressings loaded with CUR and DPA also showed the best outcomes for all the evaluated parameters: (i) epithelisation, (ii) inflammatory reaction, (iii) proliferation rate of fibroblast and (iv) neoangiogenesis.

1. Introduction

The interest in 3D printing (also known as additive manufacturing) for pharmaceutical and biomedical applications has increased significantly during the last decade [1,2]. A wide variety of formulations and medical devices have been prepared using 3D printing technology such as: tablets [3–5], capsules [6], suppositories [7], wound dressings [8,9] surgical instruments [10,11] or implantable devices [12–14] among many others. 3D printing is an umbrella term that includes a wide variety of techniques [15]. Recently, one of these techniques, semi-solid extrusion (SSE) (also known as robocasting) has gained attention for its potential pharmaceutical and biomedical applications [16,17]. This technology is used to combine polymers and drugs in a simple way that does not require the preparation of drug loaded filament [5,18,19] and

* Corresponding authors.
E-mail addresses: j.dominguezrobles@qub.ac.uk, jdominguez6@us.es (J. Domínguez-Robles), nrmorcas@uis.edu.co (N. Moreno-Castellanos), e.larraneta@qub.ac.uk (E. Larrañeta).

https://doi.org/10.1016/j.susmat.2023.e00581
Received 11 August 2022; Received in revised form 8 December 2022; Accepted 30 January 2023
Available online 3 February 2023

can be used to load relatively high drug loadings [20,21]. A potential area of application of robocasting is the preparation of wound dressings [22].

One of the critical needs for wound dressings is to accelerate wound healing while preventing bacterial infection. The use of wound dressings loaded with antimicrobial compounds has been gaining attention [23,24]. Therefore, 3D printing can be used to prepare personalised wound dressing with antimicrobial properties. Additionally, it has been reported that antioxidant compounds contribute to controlling oxidative stress in wounds, accelerating their healing [25,26]. A large selection of antioxidant molecules can be found in nature, two such compounds being lignin (LIG) and curcumin (CUR). Interestingly, these two compounds present both antioxidant and antimicrobial properties [27,28].

LIG is a natural polymer that can be found in vascular plants [29]. This biopolymer provides mechanical and chemical protection to the plants [28,30]. Additionally, LIG has been reported to present antimicrobial and antioxidant properties [31–35]. Therefore, LIG has potential to be used in wound healing applications. This is particularly interesting considering its availability as after cellulose, LIG is the second most abundant polymer on the planet [29,36]. This product is a by-product of paper manufacturing and normally is used as energy source or simply treated as a waste [37,38]. Despite these properties, less than 2% of the total production of LIG is used to prepare products [37,39,40]. Therefore, there is a clear need of finding alternative uses for LIG. In recent years, researchers have been working on preparing a wide variety of materials containing LIG for biomedical applications [32,35,41–43].

CUR is a natural molecule that can be found in turmeric (*Curcuma longa*) [44]. CUR present similar properties to LIG as it is an antioxidant, anti-inflammatory and antimicrobial compound [45]. Additionally, CUR has wound healing properties [45]. In addition to CUR and LIG, there are other compounds that could be highly beneficial for wound healing such as D-Panthenol (DPA). This molecule improves epidermal regeneration by boosting lipid synthesis, epidermal differentiation and promoting human skin fibroblast proliferation [9,46,47] while providing a moisturising effect to the skin [46,48].

In this work we propose the use of LIG, CUR and DPA combined with poly(caprolactone) (PCL), thus maximising the effect of the formulations to prepare 3D-printed wound dressings by using SSE 3D printing technology. The resulting implants were characterised through multiple techniques such as Fourier transform infrared (FTIR) spectroscopy, thermal analysis, X-ray diffraction (XRD) and optical/electronic microscopy. Subsequently, the release of CUR and DPA from the wound dressings was evaluated. Moreover, the biocompatibility, antimicrobial and antioxidant properties of the resulting materials were evaluated. Finally, the efficacy of the 3D-printed wound dressings was evaluated using a rat animal model. The results presented in this work highlights a potential area of exploitation for LIG-based materials. PCL has been used in the past for the preparation of 3D-printed wound dressings [23,24]. However, to the best of our knowledge, this is the first work describing the combination of LIG/CUR/DPA for wound healing applications.

2. Materials and methods

2.1. Materials

Two different forms of PCL, CAPA™ 6506 (M_W = 50,000 Da, *i.e.*, high molecular weight), henceforth referred to as H-PCL, and CAPA™ 2054 (M_W = 550 Da, *i.e.*, low molecular weight), henceforth referred to as L-PCL, were both provided by Perstorp (Malmö, Sweden). LIG sample (BioPiva 190) was a softwood kraft LIG acquired by UPM (Helsinki, Finland). Both CUR (95%) and DPA (≥98%) were purchased from Alfa Aesar by Thermo Fisher Scientific (Lancashire, UK). Tween 80 (reagent grade) and phosphate-buffered saline (PBS) tablets to prepare PBS solution (pH 7.0) were both obtained from VWR (Lutterworth, UK). DPPH (2,2-diphenyl-1-picrylhydrazyl) was provided by Sigma Aldrich (Dorset, UK). Additionally, L-ascorbic acid E300 (ultrafine) was provided by DSM (Heerlen, the Netherlands). All materials and reagents were used as received. Tryptone soya broth (TSB), quarter-strength Ringer's solution (QSRS) and Mueller-Hinton (MH) broth were obtained from Oxoid Ltd. (Hampshire, UK). *Staphylococcus aureus* NCTC 10788 was maintained in glycerol at −80 °C and cultivated in MH broth at 37 °C and at 100 rpm when required for the microbiological assessments.

2.2. 3D-printed wound dressings design and manufacture

Wound dressings were designed using computer-aided design (CAD) software and printed using a 3D bioprinter (Bioscaffolder 3.2, GeSiM) (Radeberg, Germany). Prior to the printing process, all of the formulations used for the manufacture of these 3D-printed materials were prepared. For this purpose, a mixture of H-PCL/L-PCL (60%/40% *w*/w) was selected as the main polymer matrix and combined with the rest of the compounds (LIG, CUR and DPA) in the defined proportions shown in the Table 1 by using the SpeedMixer™ DAC 150.1 FVZ-K (Hauschild GmbH & Co. KG, Westfalen, Germany) at 3500 rpm for 5 min. Moreover, the abovementioned ratio of H-PCL/L-PCL was chosen due to its 3D printing suitability, when up to 20% of bioactive compounds are loaded in the PCL-based matrix, as previously reported [20,21]. Then, the formulations were placed into the metal cartridge of the 3D bioprinter, ready to be printed. The 3D BioScaffolder system was equipped with a 0.5 mm nozzle. The print speed used to 3D print the wound dressings (circular meshes of 10 mm diameter) was 10 mm/s, the print temperature used was 60 °C and the layer height and strand distance were 0.25 mm and 1.4 mm, respectively. Moreover, discs (circles of 13 mm diameter) were designed and 3D-printed to characterize the 3D-printed materials. For this purpose, the strand distance was set at 0.65 mm, the rest of the parameters remained the same.

2.3. 3D-printed wound dressings characterisation

2.3.1. Microscopy

The surface morphology of the designed 3D-printed samples was evaluated by using scanning electronic microscopy (SEM) (Hitachi TM3030; Tokyo, Japan) and a Leica EZ4 D digital microscope (Leica, Wetzlar, Germany). Moreover, the SEM micrographs were analysed using the imaging software ImageJ® (National Institutes of Health, Bethesda, USA) in order to measure the pore size of the different 3D-printed samples.

2.3.2. Fourier transform infrared (FTIR) spectroscopy

The FTIR spectra of the 3D-printed samples and the pure compounds were recorded using a Spectrum Two™ instrument (Perkin Elmer, Waltham, MA, USA) by the attenuated total reflectance (ATR) technique to evaluate if any interactions had taken place between the different drugs and polymeric compounds. For this purpose, the resulting spectra were recorded at a room temperature from 4000 to 600 cm^{-1} with a resolution of 4 cm^{-1} and a total of 32 scans were collected.

2.3.3. X-ray diffraction (XRD) analysis

The crystalline structure of the 3D-printed samples was evaluated by XRD analysis. This assay was carried out using MiniFlex II Dekstop Powder X-ray diffractometer (Rigaku Corporation, Kent, UK). The test

Table 1
Wound dressing formulations.

Formulations	PCL mixture (%) H-PCL (60%)/L-PCL (40%)	LIG (%)	CUR (%)	DPA (%)
PCL	100	–	–	–
10% LIG	90	10	–	–
5% CUR	85	10	5	–
5% DPA	85	10	–	5
5% CUR_5%DPA	80	10	5	5

conditions were set to be Cu Kβ XRD source, accelerating voltage 40 kV, acceleration currency 15 mA, scan rate 2.0°/min, scan step 0.03° and scan range 5–60° 2Θ (2 theta) at room temperature [49].

2.3.4. Thermal analysis

Thermal properties of the 3D-printed materials, pristine polymers and the pure drugs were evaluated by performing thermogravimetric (TGA) and differential scanning calorimetry (DSC) analyses. As the materials were subjected to moderate temperatures (60 °C) during the 3D printing process, the thermal behaviour of the polymer mixtures, with and without drug molecules, were examined. For this purpose, small pieces of the 3D-printed materials (between 3 and 10 mg) were used. TGA was performed using a Q50 Thermogravimetric analysis (TA instruments, Bellingham, WA, USA). Samples were heated at a rate of 10 °C/min from room temperature to 500 °C under a nitrogen flow rate of 40 mL/min. Additionally, a Q20 differential scanning calorimeter (TA instruments, Bellingham, WA, USA) was used to evaluate drug-polymer interactions and establish if CUR formed an amorphous dispersion after mixing with the polymer matrix. For this purpose, CUR powder and small pieces of 3D-printed materials (between 3 and 10 mg) were analysed from 30 °C to 300 °C at a heating rate of 10 °C/min, under a nitrogen flow rate of 50 mL/min.

2.4. Antioxidant properties

DPPH radical was employed to measure the antioxidant activity of 3D-printed materials based on the radical scavenging property of the LIG and CUR [31,35,50]. Briefly, 5 mL of a DPPH solution dissolved in methanol (50 mg/L) was added to the 3D-printed samples (circles of 13 mm diameter) placed in a vial. A control sample of 50 mg/L of DPPH in methanol was also measured. The samples were then incubated for 30 min at room temperature in a dark environment. At predetermined time intervals (15 and 30 min), 300 μL solution was collected and the vials were immediately replenished with an equivalent volume of methanol. The absorbance of the different solutions was measured at 517 nm using a UV–vis plate reader (PowerWave XS Microplate Spectrophotometer, Bio-Tek, Winooski, VT, USA) ($n = 4$). Radical DPPH scavenging capacity was calculated using the Eq. (1).

$$\text{Residual DPPH content } (\%) = 100\text{–}100\ (A_0 - A_1/A_0) \quad (1)$$

where A_0 is the absorbance of the control sample and A_1 is the absorbance in the presence of the sample at any time. Decreased absorbance of the reaction indicates a stronger DPPH radical scavenging activity.

2.5. Antimicrobial properties

The *in vitro* microbiological analysis was performed according to the previous published works [51,52]. A bacterial suspension of *S. aureus* (1×10^8 cfu mL^{-1}) in PBS was diluted 1 in 100 with PBS containing 0.5% TSB. Replicate samples of the 3D-printed specimens (circles of 13 mm diameter) were placed in individual wells of a 24-well flat bottom tissue culture plate and then 1 mL aliquots of the bacterial suspension with a density of 1×10^6 cfu mL^{-1} were added, ensuring the 3D-printed specimens were completely covered. The plate was continuously shaken at 100 rpm in an orbital incubator at 37 °C for 4 and 24 h. Then, the samples were removed from the tissue culture plate using sterile forceps, and the non-adherent bacteria were removed by serial washing for 1 min, first in PBS (2×10 mL), and secondly, in QSRS (2×10 mL). After this washing step, 3D-printed specimens were transferred into fresh QSRS (5 mL), and then adherent bacteria were subsequently removed by sonicating for 15 min in an ultrasonic bath and vortexing for 30 s. The sonication technique has previously been demonstrated not to affect bacterial viability or morphology [53]. A viable count of the QSRS was performed by the Miles and Misra serial dilution technique [54], followed by plating onto Mueller-Hinton agar to determine the number of adherent bacteria on each 3D-printed specimen surface. Percentage reductions in adherence of *S. aureus* relative to the pristine PCL control were calculated.

2.6. In vitro drug release studies

An *in vitro* release study was performed to calculate the amount of drug eluting from the resulting 3D-printed wound dressings (circular meshes of 10 mm diameter). The 3D-printed wound dressings were weighed and placed in watertight glass vials containing 50 mL of dissolution medium (PBS pH 7.0 containing 0.5% *w*/w Tween 80 and 0.1% w/w L-ascorbic acid) to maintain sink conditions. Subsequently, these vials were placed in a shaking incubator of simulated body temperature conditions (37 °C), shaking at a rate of 40 rpm. At specific time points, the 3D-printed wound dressings were removed from the bottles, dried, and transferred to new bottles containing 50 mL of fresh dissolution medium. The concentration of drugs was quantified using high-performance liquid chromatography (HPLC).

2.7. Instrumentation and chromatographic condition for analytical method

The analysis of CUR and DPA in the *in vitro* drug release studies were conducted using HPLC instrument (Agilent Technologies 1220 Infinity UK Ltd., Stockport, UK) with the method validated as per guidance from the International Committee on Harmonisation (ICH) 2005 [9]. The separation of analytes was carried out using an XSelect CSH C18 column (3.0×150 mm with 3.5 μm particle size) (Waters, Dublin, Ireland). The injection volume was 20 μL, the flow rate was 0.8 mL/min, with the analyses performed at room temperature. The mobile phase consisted of a mixture of 0.001% *v*/v of phosphoric acid in water (part A) and acetonitrile (B). A gradient condition was used to separate the analytes as detailed in Table 2.

2.8. Biocompatibility assays

2.8.1. Cell culture and scaffold seeding

Mouse fibroblast cell line (3 T3-L1 ATCC CL-173) was cultured in DMEM (Sigma-Aldrich, Saint Louis, USA) with 17.5 mM glucose, 1% antibiotic-antimycotic (*v*/v) solution (Sigma-Aldrich, Saint Louis, USA), 4 mmol/L L-glutamine, 1.5 g/L sodium bicarbonate and supplemented with 10% foetal bovine serum (FBS) (*v*/v) (Sigma-Aldrich, Saint Louis, USA). Cells were seeded at a density of 2×10^5 cell/cm^2 and incubated at 37 °C/5% CO_2 until they reached 80% confluence. 3D-printed scaffolds were sterilised with UV-253 nm for 15 min and then placed into a 24-well plate. The cells were dispersed with 0.25% (*w*/*v*) trypsin-0.53 mM EDTA solution, seeded on the structures at a density of 3×10^3 cell/cm^2 and were finally incubated for 3 days at 37 °C/5% CO_2.

2.8.2. Viability assessment

Cell viability was measured by an MTT (3-(4,5-dimethylthiazol-2-yl)-2,5-diphenyl tetrazolium bromide) (Sigma-Aldrich, Saint Louis, USA) assay as previously described [55–57]. After 3 days of culture, 0.5 g/L of MTT stock solution was added to the wells containing the cells with/without a 3D-printed scaffold and incubated for 5 h until crystals had formed. After this stage, the wells were washed with phosphate buffered saline (PBS) solution (pH 7.2) and crystals were diluted with

Table 2
Gradient condition for separation and simultaneous quantification of CUR and DPA.

Time (min)	A (%)	B (%)	Wavelength (nm)
0–7	94	6	200
7–12	25	75	435
12–15	94	6	200

dimethyl sulfoxide (DMSO) (Sigma-Aldrich, Saint Louis, USA). The absorbance was recorded at 570 nm using a Sinergy H1 microplate reader (Agilent technologies, St, Clara, USA). The control positive used in this assay was fibroblast cells seeded with no tested materials, and Triton X-100 (1%) was used as a negative control.

2.8.3. Lactate dehydrogenase release assay

To assess the cytotoxic activity of scaffold evaluating the percentage of membrane 3D-printed scaffold cell rupture, lactate dehydrogenase (LDH) activity (Sigma-Aldrich, Saint Louis, USA) assay was carried out. The cells were resuspended in DMEM after a PBS wash, an amount of 50 μL of the cells suspensions was treated with 50 μL of 2% (*v*/v) Triton X-100 in PBS for 30 min at 37 °C. Afterwards, 100 μL of lysed cell solution from each well was transferred into 100 μL LDH substrate in a 96-well plate. A standard curve to interpolate the LDH activity was also made, followed by a 30 min incubation in the dark. Absorbance measurements at 450 nm were taken following this period.

2.8.4. Proliferation assay

PicoGreen® (Invitrogen, Thermo Scientific, Waltham, MA, USA) assay was used to evaluate cell proliferation for all the 3D-printed scaffold conditions following the manufacturer's guidelines. A standard curve of known DNA concentrations was made to determine DNA content. After 5 min of room temperature incubation, sample fluorescence was read on a Synergy H1 microplate reader (Agilent technologies, St, Clara, USA) with an excitation at 480 nm and emission at 520 nm.

2.9. Wound size measurements in an animal model

Animal studies met the corresponding International and National guidelines under the approval of The Committee on Ethics in Scientific Research of the Universidad Industrial de Santander (CEINCI-UIS, approval number 4110, August 2020). A model for inflicted wounds was used to assess the effect of the 3D-printed dressings on the wound healing process in rats [58,59]. Healthy, adult Wistar albino male rats were randomly selected and divided into five groups: control group (CTRL) without using a 3D-printed dressing, 3D-printed dressing manufactured from PCL (PCL), PCL and 10% LIG (10% LIG), PCL, 10% LIG and 5% CUR (5% CUR) and PCL, 10% LIG, 5% CUR and 5% DPA (5% CUR_5%DPA) (Table 1). Every group had at least six animals ($n \geq 6$), of which three animals were sacrificed at day 7 and the other three sacrificed at day 13, for wound size measurements and histology assay. Briefly, male adult rats were sedated with xylazine 2% (Erma laboratories, Funza, Colombia) and anesthetised before the procedure with ketamine 50 mg/mL (Holliday-Scott S.A., Buenos Aires, Argentina). The back of the rats was shaved and cleaned, ensuring no unnecessary damage to the skin, and a single circular wound to a diameter of ~8 mm was made with a circular mould (8 mm diameter), a scalpel strip and scissors under aseptic conditions on the back of each animal for every experimental group. The circular skin portion was taken out, and then the 3D-printed dressing was placed and sutured over the wound. Moreover, the single wounds and 3D-printed dressings were protected with sterile gauze to avoid auto-mutilation, and removal of the dressings. The animals were placed in single cages upon surgery for recovery. A meloxicam 0.15% solution was given to each rat for five days as an analgesic. Food and water were given *ad libitum* and the photographic registration was made on the lapse of 13 days.

Pictures of the wounds were taken on days 0, 7, and 13. Images were analysed, and the wound area was accurately calculated using densitometric analysis with the calibrated image to a set scale with ImageJ v. 1.53. (NIH, USA) software. The relative wound area was calculated using the Eq. (2).

$$\%\text{Wound size} = [(\text{Day X Wound area})/\text{Day 0 Wound area}] \times 100 \quad (2)$$

where day 0 is the initial wound area and day X is the wound area at different time periods.

2.10. Histological evaluation

Rats of each experimental group were sacrificed by CO_2 inhalation on seven and thirteen days after surgery. The wound dressings were gently detached, liberating the sutures to expose the healed skin on day 7 and 13 before analysis. The skin wounds were removed from the body and processed as described before [60] to histology assay. Briefly, the skin covered by new hair in the proximity of the wounds was shaved to avoid contamination. The tissues recollected were fixed in 10% buffered formalin without rinsing them in another solution (Sigma-Aldrich, Saint Louis, USA) and embedded in paraffin (Sigma-Aldrich, Saint Louis, USA). The biopsies were sectioned into 5 μm thick slices. They were stained with haematoxylin-eosin (Sigma-Aldrich, Saint Louis, USA) and examined under an optical microscope (Leica DM500, Wetzar, Germany). A semi-quantitative method was used to perform the following analyses: (i) epithelisation (measure of the keratinocytes migration to fill the excision), (ii) PMNL (presence of polymorphonuclear leukocytes-inflammatory cells infiltrated in the surrounding granulation tissue, and at the demarcation line), (iii) fibroblasts (presence of fibroblast in the granulation tissue and surrounding tissues), and (iv) formation of new vessels (presence of capillaries formed by endothelial cells in the subcutaneous and granulation tissue). The scale used to assess is as follows: in the epidermis (parameter i) (0 - thickness of cut edges, 1 - migration of epithelial cells (<50%), 2 - migration of epithelial cells (>50%), 3 - bridging of the incision, 4 - complete regeneration/keratinization), in the dermis or striated muscle layer (parameters ii, iii, iv) (0 - absent, 1 - mild surrounding tissue, 2 - mild demarcation line or granulation tissue, 3 - moderate demarcation line or granulation tissue, 4 - marked demarcation line or granulation tissue) [61,62]. Digital images were evaluated by one independent observer blinded to the treatment groups. Semi-quantification of parameters was conducted using ImageJ v. 1.53. software (NIH, USA).

2.11. Statistical analysis

All quantitative data were expressed as a mean ± standard deviation, or ± standard error of the mean, in the case of *in vivo* assays. Statistical analysis was performed using a one-way analysis of variance with Tukey's post-hoc. For the release study, an unpaired *t*-test was used to compare the release values of CUR from the 3D-printed dressings, when this compound was alone or in combination with DPA.

3. Results and discussion

3.1. Preparation and physicochemical characterisation of 3D-printed samples

PCL/LIG-based wound dressing (circular meshes of 10 mm diameter) containing 5% CUR and/or 5% DPA were manufactured using semi-solid extrusion (SSE) technology (Fig. 1), which is a 3D printing process that works in a similar way as fused filament fabrication (FFF). A PCL mixture containing both H-PCL (60% *w*/w) and L-PCL (40%) was used as the main polymer matrix. This PCL mixture has been previously used to 3D print different medical devices, showing not only excellent printability properties, but also the sustainability of the 3D printing technology as the use of organic solvents are not required [20,21]. These organic solvents, commonly employed in other manufacturing techniques, such as electrospinning, can be highly flammable, harmful to humans, or entail potential issues in disposing [20,63]. Moreover, a purified softwood kraft LIG (10% *w*/w) was added, due to its antioxidant, antimicrobial properties [43] and the capacity to sustain the release hydrophobic drugs [32,41]. Kraft pulping process is the predominant pulping method and thus the major contributor to the

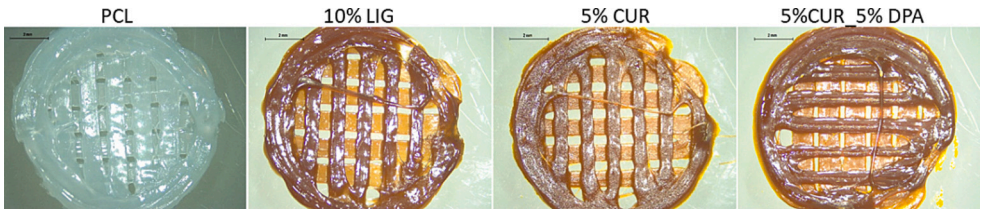

Fig. 1. Light microscope images of the 3D-printed wound dressings containing different proportions (*w*/w) of all the compounds. Scale bar is 2 mm.

availability of LIG worldwide [64].

CUR has been widely used as a wound healing agent due to its significant wound healing properties [44]. Additionally, DPA has found to be effective in supporting skin regeneration by enhancing epidermal differentiation and facilitating wound healing [65]. Moreover, DPA is a well-known moisturizer and can act as skin barrier enhancer [66,67]. The meshes were evaluated using a light microscope (Fig. 1). The addition of LIG (10% *w*/w) provided a clear darker brown colour with distinctive yellow/orange notes when CUR was added (5% w/w). Furthermore, it can be inferred that both CUR and DPA were successfully mixed within PCL/LIG matrix. This can be corroborated by light microscopy images (Fig. 1), which show complete homogeneity with no visible drug aggregates. These results suggest that complete mixing had taken place by using a dual asymmetric centrifugal laboratory mixer system and the 3D printing process itself. The good miscibility between both polymers CUR and LIG, and PCL can be explained by their chemical structures. CUR is a molecule that contains two aromatic rings and two hydroxyl groups, thus hydrogen bonding might be formed between the polymer chains and CUR [68]. Moreover, LIG is a molecule rich in aromatic rings, which could potentially interacts with the ones containing in the CUR molecule [32]. The latter interaction has been extensively reported in the literature [69].

SEM was also used to evaluate the miscibility between both polymers and CUR. SEM images of the 3D-printed samples (Fig. 2) showed no visible drug crystals or aggregates on their surfaces, thus corroborating the previously discussed outcomes found by using the light microscope. Moreover, SEM was used to assess and characterize the morphology of the surface of the 3D-printed samples. As observed in Fig. 2, the samples containing only a PCL matrix presented a smooth and quite homogeneous surface. However, when LIG is added, the surface of the 3D-printed samples was still quite homogenous (showing a good integration of the drug and the polymers), but containing a high porosity. The pore size ranged from 0.47 ± 0.14 μm (5% CUR samples) to 1.56 m ± 0.69 μm (5% CUR_5%DPA samples). Although all the 3D-printed samples presented a porous surface, the ones containing both drugs, CUR and DPA exhibited higher pore size ($p < 0.05$). Surface morphology can be affected by the drug concentration, as has been previously reported in the literature [18]. It has been reported that high porosity and highly interconnected pore structures are indeed desirable properties for scaffolds, since these materials could mimic naturally occurring tissue structures, allowing cell-cell communication as well as facilitating gas and nutrient exchange for cell proliferation [70], and thus, contributing to enhance the final outcomes of the 3D-printed dressings.

FTIR analysis was performed to evaluate any potential interactions between polymers and drugs within the samples. The obtained FTIR spectra of the different pristine compounds and 3D-printed samples are presented in the Fig. 3A. The spectra of the pristine PCL 3D-printed samples showed characteristic peaks at 2942 cm^{-1}, 2866 cm^{-1} and 1723 cm^{-1} that can be assigned to the $–CH_3$ asymmetric stretching, $–CH_3$ symmetric stretching and –C=O stretching, respectively, as previously reported in the literature [20,71]. Moreover, the FTIR spectrum of LIG showed several characteristic peaks such as the one found at 1515 cm^{-1} that can be assigned to the vibrations of aromatic rings [72]. Additionally, CUR exhibited its signature peaks at 1626 cm^{-1} and 1602 cm^{-1} that can be assigned to the aromatic moiety C=C stretching and benzene ring stretching vibrations, respectively [73,74]. These characteristic peaks for both LIG and CUR can be found in the IR spectrum of 3D-printed samples containing these compounds. When evaluating the 3D-printed samples, no new peaks were found, thus these outcomes suggest that no chemical reactions took place during the mixing or 3D printing processes.

Fig. 3B exhibits the XRD analyses of pure CUR, pure LIG, and the different 3D-printed samples detailed in Table 1. The results show that all of the 3D-printed samples presented the characteristic peaks of PCL (21.96° and 24.26°). It was shown that no CUR peaks were distinguished from all the diffractograms of 3D-printed samples. These results are thus corroborating the interaction and inclusion of CUR within the PCL/LIG polymer matrix, which has been previously reported in Dip-coated PCL coatings for titanium implants [75]. In order to further investigate the results obtained from the XRD diffractograms and evaluate the possible interactions between the polymers and loaded drugs, a thermal analysis was conducted. Thermal analysis was conducted to evaluate the possible

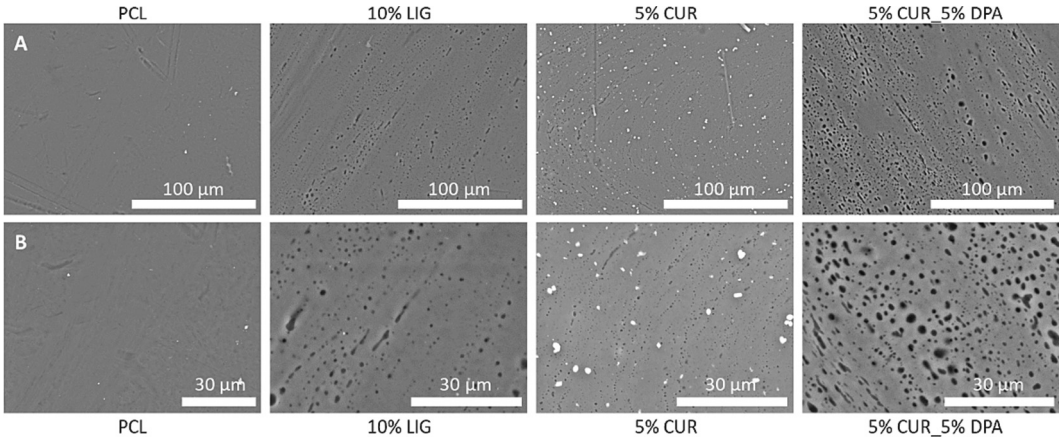

Fig. 2. SEM images of the surface of the 3D-printed wound dressings containing different proportions (*w*/w) of all the compounds (A). Higher magnification of the previous conditions (B). Scale bars are 100 μm and 30 μm, respectively.

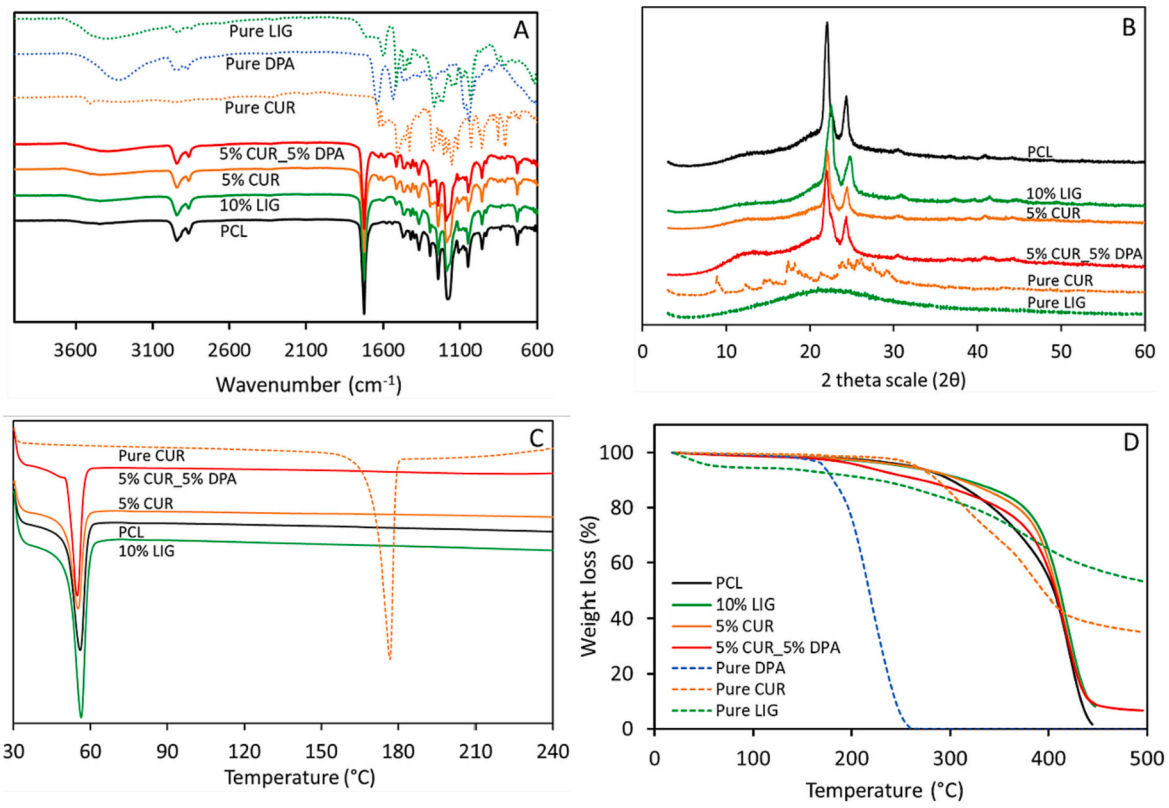

Fig. 3. ATR-FTIR spectra (A), XRD diffractograms (B) and DSC (C) and TGA curves (D) of each of the 3D-printed material composites containing different proportions (*w*/w) of all the compounds.

interactions between the polymers and loaded drugs. DSC analysis showed that when CUR was incorporated to the PCL/LIG-based polymer matrix, the sharp and endothermic melting point of CUR at around 176.76 °C was not observed (Fig. 3C). These results suggest that CUR is interacting within the PCL/LIG matrix and, thus, the crystalline form of the pure drug is converted to the amorphous form after been combined with the polymer matrix. Similar outcomes have been previously reported not only for CUR [32], but also for other types of drugs such as dipyridamole [20] or acetylsalicylic acid (ASA) [21]. Therefore, these results also corroborate the previously stated drug-polymer interactions. Furthermore, all the 3D-printed samples showed the characteristic endothermic melting point of PCL at around 56 °C (Fig. 3C), as reported in the literature [76]. However, this melting point slightly changed by one degree either higher or lower than that of PCL, when the rest of the compounds were added to the formulations.

To further investigate these interactions between PCL, LIG and both drugs, TGA analysis was also performed (Fig. 3D). Prior to the analysis of the 3D-printed samples, both drugs were analysed using TGA to ascertain their thermal stability, as the material was subjected to a moderate temperature (60 °C) during the 3D printing process. As can be observed in Fig. 3D, DPA and CUR were both stable at 60 °C. LIG showed an initial small weight loss (around 5.5% of the total weight) due to the water content, and after this stage the LIG began to degrade slowly from approximately 190 °C to 210 °C, as reported in the literature [30,77]. Moreover, DPA is more thermolabile than CUR (266 °C) or PCL mixture (261 °C) as it started degrading at temperatures around 172 °C. Thus, this would explain that 3D-printed samples containing DPA showed a lower T_{onset} (212 °C) than the blank (PCL mixture) 3D-printed samples. Additionally, the rest of the 3D-printed samples containing 10% LIG (10% LIG), and 10% LIG and 5% CUR (5% CUR) showed similar T_{onset} of 254 °C and 257 °C, respectively.

3.2. Antioxidant properties of 3D-printed materials

Reactive oxygen species (ROS) play a crucial role in the mobilisation of the normal wound healing response [78]. In order to evaluate the antioxidant properties of the 3D-printed dressings, a DPPH assay was carried out (Fig. 4). Although PCL matrix showed minimal antioxidant activity, reducing the DPPH concentration up to *ca.* 27% after 30 min, the dressings containing 10% LIG or 10% LIG and 5% CUR were able to remarkably reduce the DPPH concentration up to *ca.* 71% and 74%, respectively, after 15 min (Fig. 4). As expected, these results indicate that the presence of LIG and CUR gave the dressings antioxidant

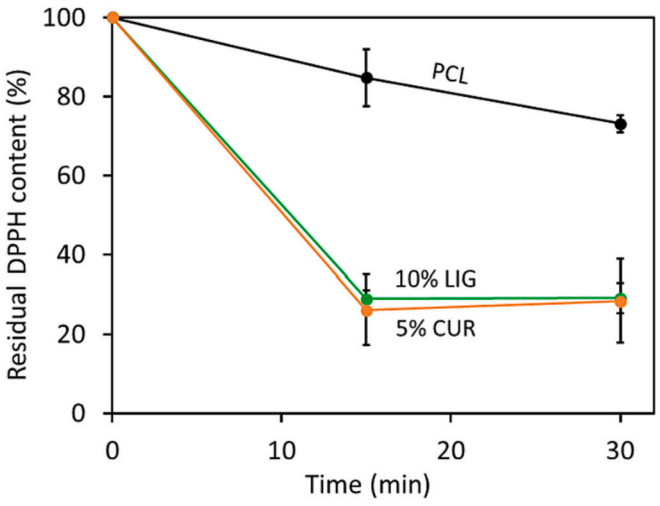

Fig. 4. Residual DPPH content as a function of time for PCL/LIG-based 3D-printed dressings using an initial DPPH concentration of 50 mg/L.

properties. Although the antioxidant properties of CUR have been previously proved in several studies [79,80], the addition of CUR (5% *w*/w) did not significantly increase the antioxidant properties of the 3D-printed materials, thus no synergistic effect was found. LIG and CUR are both well-known antioxidant compounds [81,82], thus, these results are in agreement with those found in the literature [35,41,83,84]. Antioxidant properties may provide added benefit to the final wound dressing. These wound management products which are able to regulate this balance are a target for new therapies [82]. Additionally, LIG can be used as protective agent in order to prevent the degradation of the drugs loaded in the dressings, as well as to modify the drug release profile [41].

3.3. Antibacterial properties of 3D-printed materials

One of the most important properties when manufacturing wound dressings, is the ability to avoid complications related with persistent infection which could lead to delayed wound healing [85]. Additionally, natural polymers such as LIG or CUR have shown enough potential as antibacterial agents [31,35,86], thus offering a new way to fight bacterial infection [87]. For instance, CUR has been already reported as an antibiotic resistance breaker against a multi-resistant clinical isolate of *Mycobacterium abscessus* [86]. Bacterial adherence to the surface of the 3D-printed samples was studied with the Gram-positive *S. aureus* as a model pathogen. Moreover, this pathogen can cause a wide variety of clinical manifestations [88]. Infections caused by *S. aureus* are common both in community-acquired and hospital-acquired settings [88].

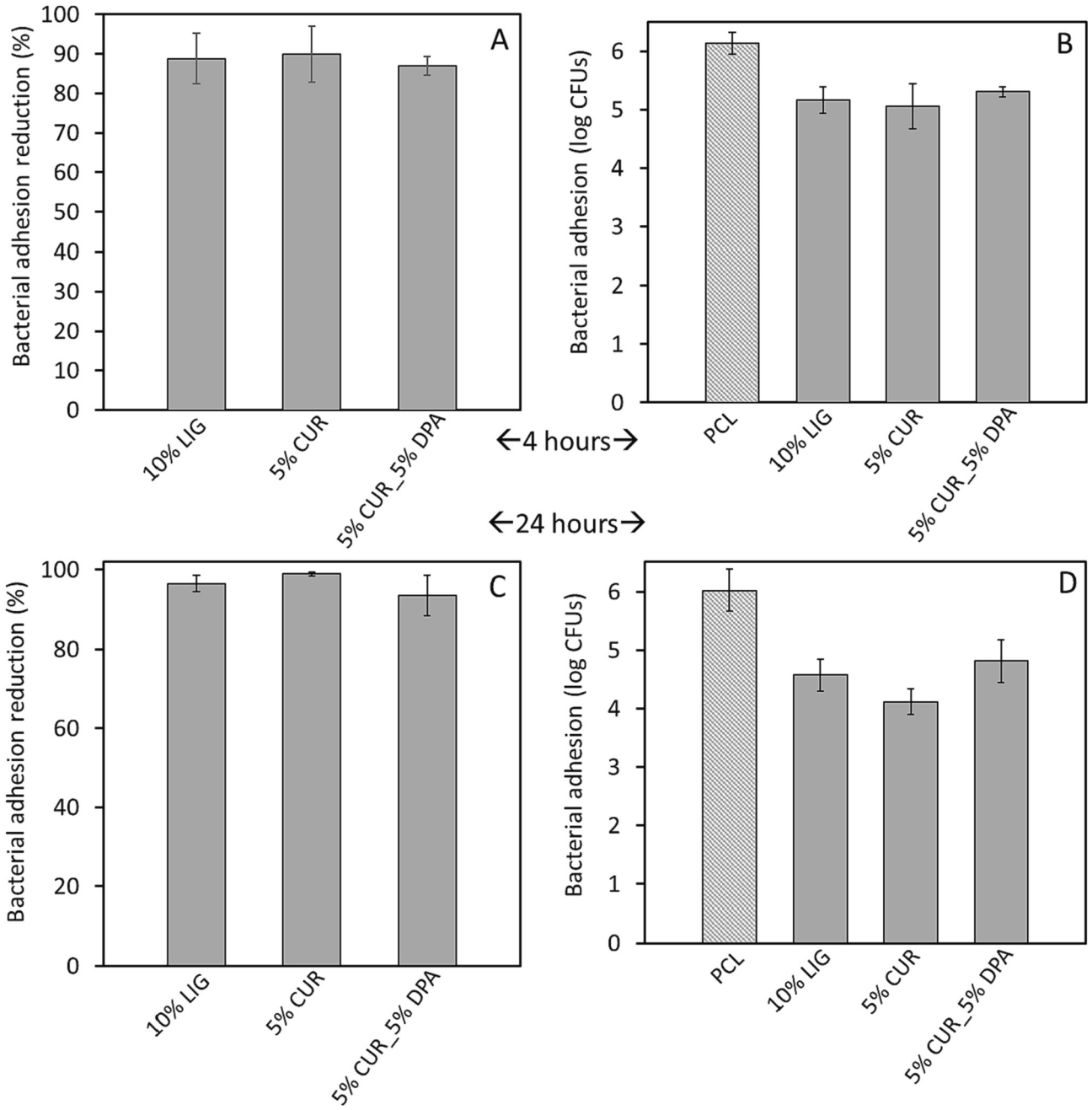

Fig. 5. *S. aureus* adhesion reduction relative to PCL control for the rest of the PCL/LIG-based 3D-printed wound dressings containing different proportions (*w*/w) of all the compounds after incubation periods of 4 h (A) and 24 h (C). *S. aureus* adhesion to PCL/LIG-based 3D-printed wound dressing after incubation periods of 4 h (B) and 24 h (D).

Moreover, this pathogen causes the most medical device-related infections [89].

3D-printed samples were tested with inoculi of *S. aureus* (1×10^6 cfu mL^{-1}) over incubation periods of 4 h and 24 h. Percentage and logarithmic reductions in the number of adherent bacteria to each 3D-printed sample relative to the PCL control (3D-printed samples containing only PCL) are presented in the Fig. 5. As noted in Fig. 5A and C, 3D-printed samples containing LIG (10% LIG), LIG and CUR (5% CUR), and LIG, CUR and DPA (5% CUR_5%DPA) showed a marked resistance to adherence of *S. aureus* when compared to the PCL control 3D-printed samples, resulting in substantial reductions of up to 88.8%, 89.9% and 86.9% after 4 h and 96.6%, 98.9% and 93.6% after 24 h of incubation periods ($p < 0.05$), respectively. Nevertheless, no significant differences were found between all the loaded samples, 10% LIG, 5% CUR and 5% CUR_5% DPA ($p > 0.05$). Moreover, all the 3D-printed samples revealed logarithmic reductions (after 4 h incubation period) equal or greater than 1 unit (after 24 h incubation period) in comparison to the PCL control samples ($p < 0.05$) (Fig. 5B and D). Additionally, after a challenged period of 24 h, those 3D-printed samples containing LIG and CUR (5% CUR) showed the greatest logarithmic reduction (around 2 units), followed by samples containing only 10% of LIG (10% LIG) (around 1.5 units), however, no significant differences were found between these two samples ($p > 0.05$) (Fig. 5D).

These results are very promising considering that anti-infective dressings have the ability to avoid complications related with persistent infection which could lead to delayed wound healing [85]. Different LIG-based materials, such LIG/poly(butylene succinate) composites (up to 15% LIG w/w) have shown marked resistance to adherence of *S. aureus* when compared to the poly(butylene succinate) control sample, resulting in significant reductions of around 90% in adherence of *S. aureus* after 24 h incubation [35]. The phenolic groups of LIG are known to damage the bacterial envelope and subsequently lead to cell lysis and release of the cellular components, thus providing antimicrobial properties to this biomacromolecule [43,90,91]. Moreover, these outcomes are indicative that the addition of CUR to the 3D-printed samples (5% CUR) demonstrated a greater efficacy in reducing adherence of bacteria to the 3D-printed samples surfaces. The antibacterial action of CUR has been extensively reported in the literature [86,92–94]. For instance, CUR has been incorporated to composite chitosan films, exhibiting significant antibacterial activity against *Escherichia coli* [92]. The antibacterial activity of this phenolic compound can be attributed to its capacity to inhibit the polymerization of filamentous temperature-sensitive protein Z (FtsZ), a protein which is necessary for cell division and bacterial sustainability [95]. Additionally, bacterial adherence to the biomaterials surface depends on many factors including chemistry, hydrophobicity and surface energy, drug loading and also on bacterial surface properties [96,97], thus it can be hypothesised that inclusion of DPA may affect at least one of these factors. Although the samples containing DPA (5% CUR_5% DPA) showed the lowest logarithmic reduction, no significant differences were found between all the loaded samples, 10% LIG, 5% CUR and 5% CUR_5% DPA ($p > 0.05$). Therefore, these antimicrobial dressings have a great potential to minimize the appearance of complications related with persistent infections when treating a wound.

3.4. *In vitro* drug release studies

The release of CUR from the 3D-printed wound dressings was studied in the presence and absence of DPA (5% CUR_5%DPA and 5% CUR samples, respectively). The 3D-printed wound dressings exhibited a prolonged release of CUR without an initial burst of drug over 35 days both in the presence and absence of DPA in the dressings (Fig. 6A-B). Incorporating both CUR and DPA into the formulations did not affect the release of CUR from the dressings ($p > 0.05$). The cumulative drug release of CUR from the dressings ranged between 6.58 and 7.09% and 81.04–88.18% in the first 6 h and 35 days, respectively. Moreover, to investigate the release profile of DPA from the 3D-printed wound dressings containing both drugs DPA and CUR, the release study was conducted over 10 days using the conditions as previously mentioned. Fig. 6C-D shows that the release profile of DPA from the 3D-printed

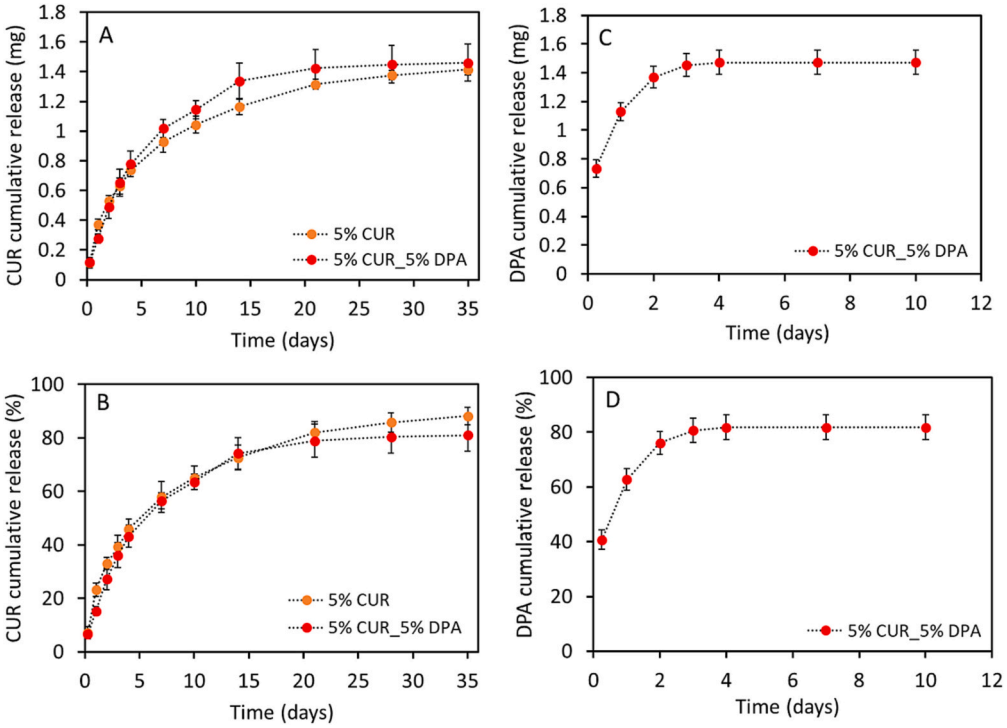

Fig. 6. *In vitro* CUR release curves from CUR-loaded 3D-printed wound dressings in PBS at 37 °C expressed in mg as function of time (A) and expressed in percentage as a function of initial CUR loading (B) ($n = 4$). *In vitro* DPA release curve from DPA-loaded 3D-printed wound dressing in PBS at 37 °C expressed in mg as function of time (A) and expressed in percentage as a function of initial DPA loading (B) (n = 4).

wound dressings presented an initial burst release, 40.73% (0.73 mg) in the first 6 h, followed by a more sustained release over a 96 h period with cumulative release of 81.79% (1.47 mg).

The differences in drug release profile between DPA and CUR are likely attributed to their solubility in water and partition in water-insoluble polymeric system [98]. DPA is a hydrophilic small drug molecule that is highly soluble in the release medium, but poorly partitions in PCL. During the fabrication, phase separation may occur rapidly between DPA and PCL, resulting in a deposition of some DPA at the surface of PCL wound dressings [99]. Hence, this leads to an initial burst release and a faster release rate when compared to CUR. Nevertheless, this 3D-printed system was able to sustain the release of DPA, a hydrophilic drug molecule, for 4 days since the interactions taking place between the polymers and the remaining portion of the drug led to a slower release rate. Similar results have already been reported in the literature [21,100]. For instance, Domínguez-Robles et al., manufactured ASA-loaded PCL-based vascular grafts by using SSE 3D printing technology, where a higher initial drug delivery was found, followed by a more sustained release [21]. In a different research work, the authors prepared 3D-printed levofloxacin-loaded thermoplastic polyurethane (TPU)-based meshes, which also exhibited a higher initial drug release for the first 24 h, followed by a more sustained release [100]. On the contrary, CUR is insoluble in water and more compatible to PCL. CUR was dissolved within the PCL matrix, with the help of the liquid L-PCL, and thus homogenously encapsulated within the PCL/LIG matrix. Similar results have already been reported in the literature [20]. Therefore, the 3D-printed wound dressings exhibited a prolonged drug release of CUR over 1 month period without a rapid burst release.

PCL has a relatively long degradation time (from months to years), however, this can be affected by several factors such as the molecular weight [76,101,102]. Therefore, the addition of L-PCL (low-molecular-weight PCL) can influence the degradation rate of the 3D-printed dressings and subsequently their release profile, as previously reported by other PCL-based materials [76,102]. For instance, Stewart et al., showed that when the proportion of L-PCL of PCL-based films was increased, the degradation rate of them was also increased [76]. Moreover, in the same study, the authors also showed that films containing the highest proportion of L-PCL showed the most rapid release, thus concluding the polymer degradation contributed to the drug release process [76].

3.5. Biocompatibility studies

Quantitative cell viability for each 3D-printed scaffold formulation was evaluated using an MTT assay. Results presented in Fig. 7A revealed that, compared to the control (plate cells culture) all the conditions were met in order to maintain viable cells. Although PCL showed the lowest cell viability, *i.e.*, 77.04 ± 4.29% ($p < 0.05$), these results are suggest that the mixture of both H-PCL and L-PCL was not cytotoxic to the fibroblast cell line [103]. Moreover, the samples containing both drugs CUR and DPA (5%DPA_5%CUR) exhibited a cell viability percentage of 147.09 ± 14.12% ($p < 0.0001$), after three days of incubation and in respect to the control. The rest of the samples did not show any significant differences in comparison to the control ($p > 0.05$). However, it is important to note that, those results confirms that all the tested conditions did not induce any toxicity to the fibroblast cell line.

In the other hand, cellular LDH release was measured to evaluate the cytotoxic effect of the biomaterials (Fig. 7B). LDH values revealed that for all treatment groups, there was a statistical significance ($p < 0.0001$) compared to the control. The addition of LIG and/or CUR helped to decrease the LDH release. However, the combination of both drugs CUR and DPA (5% CUR_5% DPA) showed the lowest LDH release proportion. Fig. 1B indicates that LDH activity tends to decrease among the groups. These findings not only corroborate the cell viability results, but also suggest there is a synergistic effect with the 5% CUR_5% DPA treatment to maintain the integrity of the fibroblast cell membrane.

PicoGreen® assay was used to assess the capability of the scaffold to induce cell proliferation (Fig. 7C). PCL and 10% LIG treatments were found to have 98.47 ± 3.53 and 95.47 ± 6.62 ng/mL, respectively with a significantly reduced level of cell proliferation ($p < 0.0001$). Moreover, the addition of CUR (5% CUR) helped to maintain the level of cell proliferation of the control (plate cells culture). However, the outcomes showed that 5%CUR_5% DPA samples were able to effectively increase fibroblasts proliferation with statistical significance ($p < 0.01$) in comparison to the control. These findings are therefore in agreement with those found in the cell viability and cytotoxicity tests reported herein.

Our biological results showed that scaffolds had good cytocompatibility, low cytotoxicity and high proliferation when cultured with 3 T3-L1 fibroblasts. This cell line was used to better correlate our *in vitro* results to the *in vivo* findings in rats, since this cell line is taxonomically similar to human cells. Initially, cell viability for PCL was found to be over 75%. According to Li et al., materials with a cell viability over 75% represent no cytotoxicity. However, statistical analysis indicated that this biomaterial alone had the lowest significant ratio compared to the control. Moreover, the LDH test revealed that PCL had a low cytotoxic effect on cells, but it must be considered that the proliferation rate was significantly lower which confirmed our viability results. Nevertheless, previous investigations have shown that PCL is a biocompatible material, which is commonly used for the development of biomedical applications [104,105]. In the case of 10% LIG, this formulation had over 80% viability which agrees with previous studies that have stated the addition of LIG may have a positive effect on cell behaviour [106–109].

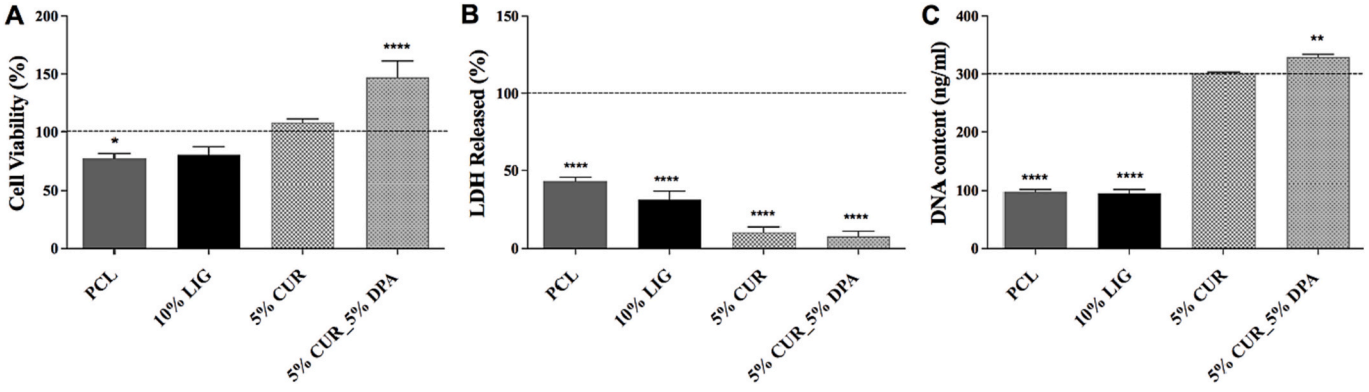

Fig. 7. Biocompatibility assays on 3 T3-L1 fibroblasts. MTT assay results show the percentage of viable cells (A). LDH release percentage of membrane 3D-printed scaffold cell rupture (B). PicoGreen assay results showing total DNA content of cells on control (cell plate culture, dotted line), PCL, 10% LIG, 5% CUR and 5% CUR_5%DPA (C). All the samples for the experiments were cultured for a period of 72 h. A standard curve of known dsDNA (ng/mL) was used to calculate the DNA content from the samples. "*, **, ***, ****" denotes a statistically significant difference ($p < 0.05$) in cell number with respect to control (plate cells culture) ($n = 3$).

Cell viability tests correlate with the low cytotoxic effect found, explained by the complex aromatic structure of the LIG, which at the same time can reduce the oxidation propagation reaction and benefit cell survival [108,110]. Our results agree with Wang et al., who demonstrated that Bone Marrow Stem Cell (BMSC) viability and cytotoxicity were gradually enhanced by different PCL and LIG combinations; however, no statistical significance was found when compared to the control group [110]. Conversely, we found there is a similar proliferation pattern as the PCL condition, suggesting that 10% LIG preparation can sustain viable cells in a non-cytotoxic medium but with a low proliferation ratio in the fibroblast cell type.

On the other hand, the formulation 5% CUR had an increasingly good viability level and a reduced cytotoxic effect. However, no significant differences were found for the proliferation state assessed for 5% CUR formulation that had a similar result as the experimental control group. In line with this, our data have suggested that the 5%CUR_5% DPA combination exhibits the greatest viability among the treatments supported by the considerably low cytotoxic effect. Furthermore, proliferation assessment allowed us to imply that fibroblasts could significantly proliferate on these 5%CUR_5%DPA scaffolds as compared to all conditions. Previous findings have found a high number of live cells where they have used DPA or CUR as stimulant agents, taking advantage of their intrinsic capabilities which have enabled the cells to adhere and survive properly [44,58,111–114]. Additionally, these favourable results may be explained because the combination of these bioactive components might have a synergistic effect in those *in vitro* assays proposing that this biomaterial may be suitable in an *in vivo* model where we expect the wound healing process would be improved [9].

3.6. Wound closure analysis

To evaluate the efficacy of the 3D-printed dressings, a macroscopic analysis was carried out and the wound healing process was measured (Fig. 8). The analysis did not show any sort of complication during the time of observation neither exudation, nor infection, or suppuration. All groups resulted in almost complete wound closure after 13 days of treatment (Fig. 8A). Wound size measurements (Fig. 8B) revealed that both PCL and 10% LIG samples had a similar feature in wound closure when compared to the CTRL, since both samples did not show any statistical significance on days 7 and 13 ($p > 0.05$). Moreover, the addition of CUR improved the wound closure, 5% CUR dressings showed significant differences when compared to the CTRL, PCL and 10% LIG dressings ($p < 0.05$), after 7 days of treatment. Additionally, 5% CUR_5% DPA 3D-printed dressings appeared to accelerate the wound closure rate in comparison to both, CTRL and PCL dressings not only after 7 days of treatment, but also after 13 days of treatment ($p < 0.05$). These results are thus suggesting that 5% CUR_5% DPA 3D-printed dressings has the best ability to accelerate the wound healing process in an *in vivo* model.

Wound size analysis revealed that there was a gradual recuperation in wound healing in all the conditions. On day 7, statistical analysis of our data showed a significant decrease in wound size for 5% CUR and 5% CUR_5% DPA treatments in comparison to the CTRL, PCL and 10% LIG dressings ($p < 0.05$). Fahimirad et al., reported that a CUR loaded PCL-based scaffold could significantly improve the wound closure in 5 days in comparison to all the groups [111]. Those results agree with these found in our study by using 5% CUR or 5% CUR_5% DPA treatments after 7 days. Moreover, the results indicated that after 13 days of treatment, the wound healing process was complete. This reflects numerous others studies that include *in vivo* models which have also used CUR or DPA [47,58,112,113,115]. Nevertheless, a stronger decrease in wound size by using both drugs together in the 5% CUR_5% DPA treatment was found in our study. Indeed, Proksch and Nissen showed the effect of DPA-containing creams reducing skin roughness and inflammation, while accelerating skin barrier repair after inducing irritation in the skin by applying sodium lauryl sulphate [48]. Thus, the outcomes found in this work may be explained by the co-active effect of the antioxidant, antibacterial and anti-inflammatory activity of this novel combination [44,108].

The results presented in this work are encouraging regarding the potential wound healing capabilities of PCL/LIG wound dressings loaded with CUR and DPA. However, it is important to remember that skin anatomy and physiology between humans and rats may be a limitation in the correlative potential for implementation in humans [116,117]. Nevertheless, a rodent standardised model is essential to provide valuable translational information due to the broad knowledge base on rat wound healing from years of extensive research [118,119]. Additionally, mesh scaffolds sutured over the wound may mimic the splint model characteristics to prevent dermal contraction and increase the relevancy of the animal model to wound healing in humans [118,120].

3.7. Histological analysis

Haematoxylin-eosin (H&E) stained images of the wounds on days 7 (Fig. 9A) and 13 (Fig. 10A) were analysed by applying a semi-quantitative score to evaluate the following parameters: (i) epithelisation, (ii) inflammatory reaction PMNL (presence of polymorphonuclear leukocytes-inflammatory cells infiltrated in the surrounding granulation tissue, and at the demarcation line), (iii) fibroblasts (presence of fibroblast in the granulation tissue and surrounding tissues) and (iv) formation of new vessels after 7 (Fig. 9B) and 13 days (Fig. 10B). Moreover, CTRL on day 0 was also analysed revealing the initiation of inflammatory reaction (see Supporting Information, Fig. S1).

After 7 days of surgery the epithelisation (measure of the keratinocytes migration to fill the excision) of open wounds for all the treatment groups was not complete (see Fig. 9B and Fig. S2 in Supporting Information). In line with this, 10% LIG and 5% CUR samples showed significant differences respect to CTRL ($p = 0.0091$ and $p = 0.0002$, respectively) and PCL samples ($p = 0.0313$ and $p = 0.0005$, respectively). However, only 5% CUR_5% DPA samples exhibited a significantly higher re-epithelisation score on day 7 in comparison to all conditions: CTRL ($p < 0.0001$), PCL ($p < 0.0001$), 10% LIG ($p < 0.0001$) and 5% CUR ($p = 0.0007$). Therefore, according to these results, DPA is accelerating wound healing through stimulating re-epithelialisation, which is in agreement with previous *in vivo* findings [46,121]. The presence of PMNL in the granulation and surrounding tissues indicate an inflammatory reaction. Interestingly, our data revealed that the dressings containing 10% LIG, 5% CUR and 5% CUR_5% DPA had greater reduction when compared with the CTRL and PCL dressings ($p < 0.05$), after 7 days of treatment. In contrast, fibroblast evaluation showed that there was a stable proliferative state, and we did not find any significant differences among the groups ($p > 0.05$), except for 5% CUR_5% DPA treatment, which had a significant difference with respect to the CTRL ($p < 0.05$), but not with rest of the conditions ($p > 0.05$). Still, rats receiving 5% CUR_5% DPA treatment showed better values at this parameter. Therefore, in addition to re-epithelialisation, valuable effect of DPA on wound healing may be the result of increased fibroblast proliferation, as previously reported by Oguz et al. [121]. Vascularisation scores were significantly increased for 10% LIG ($p = 0.0060$), 5% CUR ($p = 0.0011$) and 5% CUR_5% DPA ($p = 0.0010$) groups respect to the CTRL. Moreover, 5%CUR and 5% CUR_5% DPA groups had significance differences respect to PCL ($p = 0.0176$ and $p = 0.0164$, respectively). Therefore, it can be established that 10% LIG, 5% CUR and 5% CUR_5% DPA 3D-printed dressings helped to promote a better vascularization of the skin tissue.

After 13 days of treatment, the regeneration of the epidermis was complete (see Fig. 10A and Fig. S3 in Supporting Information) in almost all the group treatments. The differentiation process was confirmed by the maturation of keratinocytes as shown using the epithelisation scores (Fig. 10B). Specifically, epithelisation scores in 5% CUR and 5% CUR_5% DPA treatments were increased, revealing significant

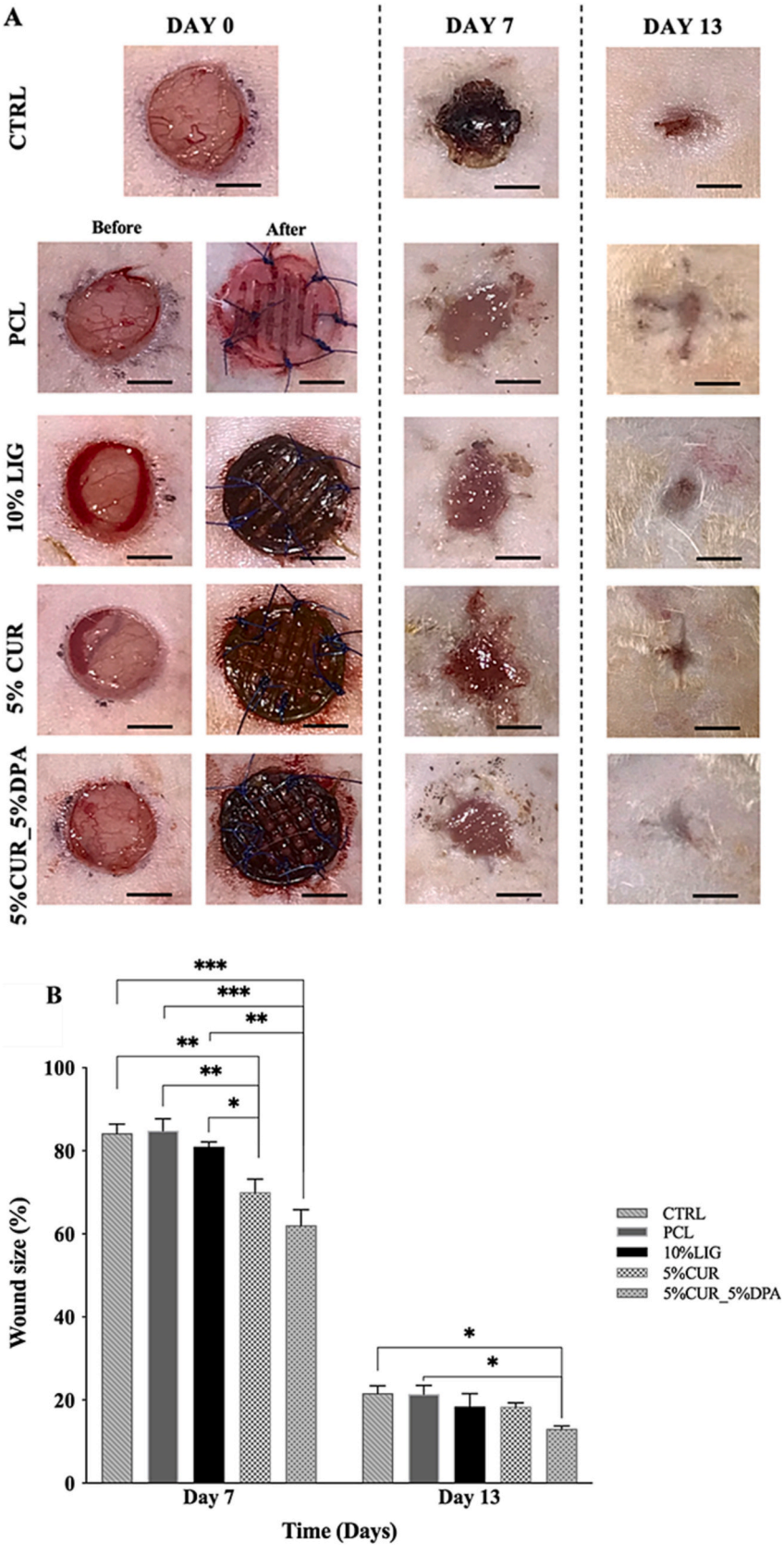

Fig. 8. Wound healing assessment on Wistar rats. Macroscopic analysis of the progress of wound healing during days 0, 7, and 13 of untreated (CTRL) and treated (3D-printed dressings sutured over the wound) rats before and after the application of examined dressings (scale bar is 5 mm) (A). Quantification of wound size calculated as percentage size compared to the original size in the presence of the different 3D-printed wound dressings (B). "*, **, ***, ****" denotes a statistically significant difference ($p < 0.05$). The values are presented as the mean ± standard error of the mean ($n = 3$).

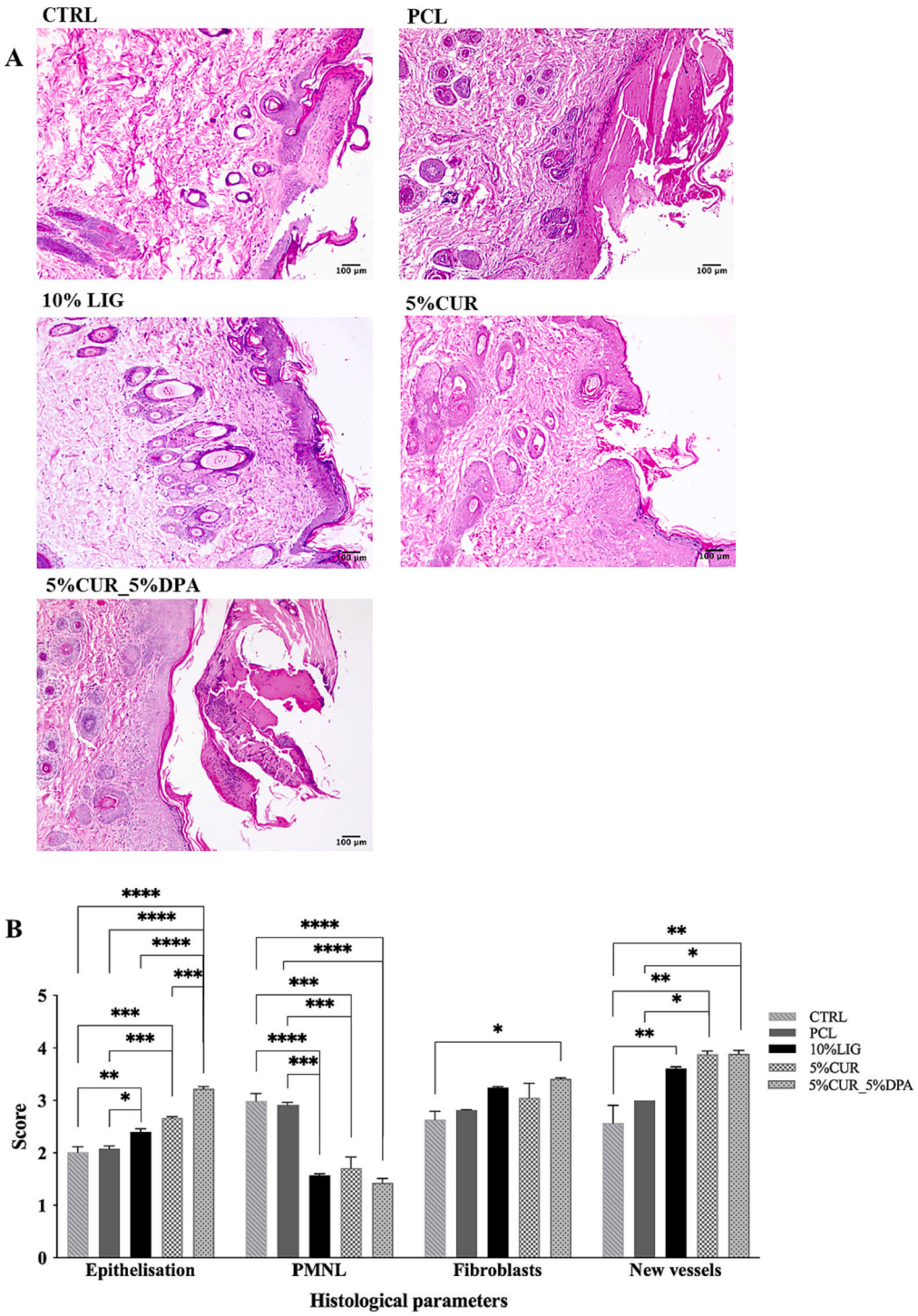

Fig. 9. Wound healing microscopic analysis with semi-quantitative assessment on day 7 after surgery for each condition and CTRL. Representative histological Haematoxylin & Eosin (H&E)-stained images of the wound sites (A). Score of histological parameters used to evaluate the wound healing process in the histological sections (B). "*, **, ***, ****" denotes a statistically significant difference ($p < 0.05$). The values are presented as the mean ± standard error of the mean ($n = 3$).

differences in comparison to the CTRL group ($p < 0.05$). Moreover, Inflammatory reaction measured by the presence of PMNL (Fig. 10B) showed that, in general terms, the inflammation reaction was lower when compared with the one found at day 7 (Fig. 9B). Additionally, the lower presence of these cells found after applying 10% LIG, 5% CUR and 5% CUR_5% DPA 3D-printed dressings in comparison to the CTRL, indicated that inflammatory process was practically finished after 13 days of treatment. Moreover, a regression in the number of fibroblasts was seen in the CTRL and PCL groups at day 13, when compared to same groups at day 7. Nevertheless, the proliferation state of fibroblasts was maintained in the other experimental groups 10% LIG, 5% CUR and 5% CUR_5% DPA. According to the angiogenesis, PCL alone did not induce this process as seen on day 7, however, the addition of LIG, CUR, or CUR and DPA maintained the degree of vascularisation respect to the CTRL after 13 days of treatment ($p < 0.05$). Moreover, in this sense, 5% CUR_5% DPA 3D-printed dressings showed a higher degree of significance when compared to the CTRL group ($p < 0.0001$).

The semi-quantitative microscopic analysis exposed that infiltration

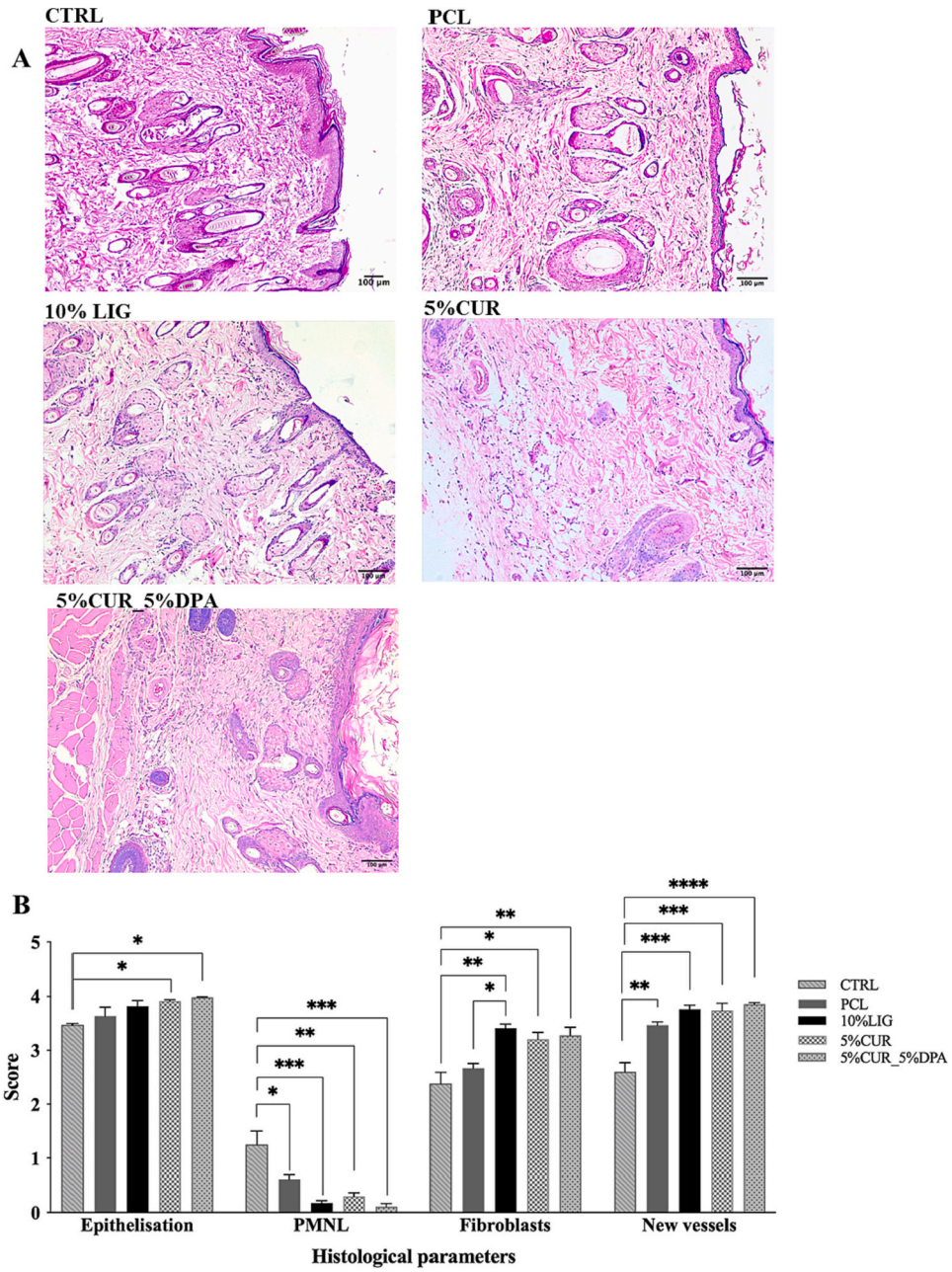

Fig. 10. Wound healing microscopic analysis with semi-quantitative assessment on day 13 after surgery for each condition and CTRL. Representative histological Haematoxylin & Eosin (H&E)-stained images of the wound sites (A). Score of histological parameters used to evaluate the wound healing process in the histological sections (B). "*, **, ***, ****" denotes a statistically significant difference ($p < 0.05$). The values are presented as the mean ± standard error of the mean ($n = 3$).

of PMNL was attenuated by all the treatments (10% LIG, 5% CUR and 5% CUR_5% DPA) when compared to the CTRL and 3D-printed dressings made only from PCL, after 7 days of treatment. The anti-inflammatory (PMNL presence) synergistic activity of these components LIG, CUR and DPA may cause the inhibition of NF-(κ)B transcription factor, reducing the production of inflammatory proteins, *e.g.*, TNF-α and IL-1 cytokines, therefore reducing inflammation. In addition, the known scavenging action against reactive oxygen species (ROS) (a major cause of inflammation) is added to the effects of these treatments. Further, the reduction of the inflammatory reaction seen in the 3D-printed dressing-loaded treatments allows the damaged skin to easily enter the later stages of wound healing [44,47,108].

On the other hand, the proliferation rate of fibroblasts in the animal model showed significant differences between the CTRL and the 3D-printed dressings containing LIG (10% LIG), LIG and CUR (5% CUR) and LIG, CUR and DPA (5% CUR_5% DPA) after 13 days of treatment ($p < 0.05$). Additionally, at this time, 10% LIG dressings also revealed significant differences in comparison with the PCL dressings ($p < 0.05$) However, some of those changes present in the skin tissue are not evident in the *in vitro* results of PCL and 10% LIG fibroblast cell line proliferation. This may be explained by the presence of different factors existing within the tissue, for instance, biological modifiers (growth factors, enzymes, and cytokines), the activity of target cells such as macrophages, and the environment of the extracellular matrix that influence positively the proliferation of fibroblasts in skin tissue [122–125]. In contrast, the 5%CUR_%DPA 3D-printed dressings helped to significantly increase proliferation when compared to the CTRL after 7 ($p = 0.0212$) and 13 days of treatment ($p = 0.0073$) not only in the *in vivo* assay, but also in the *in vitro* assay ($p = 0.0046$). These outcomes are thus indicative that even when the proliferative factors are not present

in the artificial environment model, these conditions stimulate proliferation of these cells, which is favourable for tissue regeneration.

Keratinisation (epithelisation) and neoangiogenesis (formation of new vessels) were also significantly improved by the addition of CUR (5% CUR) and both CUR and DPA (5% CUR_5% DPA) after 7 and 13 days of treatment. According to the macroscopic (Fig. 8A) and microscopic analyses as well as the score of histological parameters (Figs. 9 and 10) the wounds healed mainly by re-epithelisation. The sutured scaffolds may serve as a circular splint to prevent dermal contraction although some level of contraction may be observed as previously suggested [116–118,120]. These results are associated with the synergistic effect of these bioactive components proposing that this biomaterial may be suitable in an *in vivo* model where we expect the wound healing process would be improved [9]. Moreover, these findings are indicating the capability of these two compounds to induce neoangiogenesis and improve keratinisation since the early stages to the end stages of the wound healing process. Nevertheless, it is also important to note that 10% LIG dressings also induced neoangiogenesis and re-epithelisation effects at the early stages (7 days) of the wound healing process. Taking all these factors into account, these novel and valuable findings may strengthen the future of 3D-printed PCL/LIG-based dressings containing both CUR and DPA (5% CUR_5% DPA dressings) as the best formulation for translational applications.

4. Conclusions

This work described the preparation, characterisation, and testing of PCL/LIG-based wound dressings loaded with CUR and DPA prepared using SSE 3D printing technology. SSE was successfully used to combine CUR, DPA and LIG with PCL in a simple way to obtain homogeneous wound dressings. These materials showed clear antioxidant and antimicrobial properties due to the addition of both natural compounds LIG and CUR. Moreover, the resulting wound dressings were capable of providing sustained release of CUR and DPA. The release of CUR was slower (35 days of release) due to its hydrophobic nature as opposed to DPA hydrophilic nature (4 days of release).

PCL/LIG-based wound dressings loaded with CUR and DPA were tested using a Wistar rat animal model to evaluate their wound healing potential, as well as their safety. The results of the *in vivo* assay showed that dressings containing both drugs exhibited marked improvements from the early to the end stages of the wound healing process. Moreover, histological examination revealed that both natural compounds LIG and CUR had a remarkable influence on the improvement of all the parameters associated with the wound healing process, such as epithelisation, low presence of PMNL, presence of fibroblast in the granulation and surrounding tissues, and formation of new vessels. Furthermore, the combination of LIG, CUR and DPA showed the best outcomes for the parameters mentioned above. Thus, the results presented in this work show the promising feasibility of the SSE 3D printing technique being utilised for the manufacture of drug-eluting wound dressings.

The outcomes found in this work are promising. Due to the simplicity of SSE, this technology can be used to prepare wound dressings on demand at the point-of-care adapted for patients' needs. Despite these promising results, there is still work to do before this can happen. For example, the results obtained in rats do not always correlate with the performance in humans. Therefore, more work is required to move this technology forward by evaluating its performance in humans. Finally, before this can happen there are still many regulatory questions that need to be addressed by regulators such as FDA or EMA about the use of 3D-printing at the point-of-care. However, this scenario is changing at a fast pace as regulators are working closely with researchers to address potential issues.

CRediT authorship contribution statement

Juan Domínguez-Robles: Supervision, Conceptualization, Methodology, Funding acquisition, Investigation, Formal analysis, Writing – original draft, Writing – review & editing. **Elias Cuartas-Gómez:** Methodology, Investigation, Formal analysis. **Sean Dynes:** Methodology, Investigation, Formal analysis, Writing – review & editing. **Emilia Utomo:** Methodology, Investigation, Formal analysis. **Qonita Kurnia Anjani:** Methodology, Investigation, Formal analysis, Writing – review & editing. **Usanee Detamornrat:** Methodology, Investigation, Formal analysis, Writing – review & editing. **Ryan F. Donnelly:** Funding acquisition. **Natalia Moreno-Castellanos:** Supervision, Conceptualization, Methodology, Funding acquisition, Writing – review & editing. **Eneko Larrañeta:** Supervision, Conceptualization, Methodology, Funding acquisition, Writing – review & editing.

Declaration of Competing Interest

The authors declare that they have no known competing financial interests or personal relationships that could have appeared to influence the work reported in this paper.

Data availability

Data will be made available on request.

Acknowledgements

This work was financially supported by the Wellcome Trust (UNS40040) and the Society for Applied Microbiology (*Sf*AM) through the funding of a summer student placement scholarship. Authors also thank to Luki Ahmadi Hari Wardoyo for designing the graphical abstract of this manuscript and Raquel Elvira-Ocazionez of the Universidad Industrial de Santander, Colombia, for infrastructure support.

Appendix A. Supplementary data

Supplementary data to this article can be found online at https://doi.org/10.1016/j.susmat.2023.e00581.

References

[1] I. Seoane-Viaño, S.J. Trenfield, A.W. Basit, A. Goyanes, Translating 3D printed pharmaceuticals: from hype to real-world clinical applications, Adv. Drug Deliv. Rev. 174 (2021) 553–575, https://doi.org/10.1016/j.addr.2021.05.003.
[2] C.L. Ventola, Medical applications for 3D printing: current and projected uses, P T. 39 (2014) 704–711.
[3] X. Xu, A. Seijo-Rabina, A. Awad, C. Rial, S. Gaisford, A.W. Basit, A. Goyanes, Smartphone-enabled 3D printing of medicines, Int. J. Pharm. 609 (2021), 121199, https://doi.org/10.1016/j.ijpharm.2021.121199.
[4] A. Goyanes, F. Fina, A. Martorana, D. Sedough, S. Gaisford, A.W. Basit, Development of modified release 3D printed tablets (printlets) with pharmaceutical excipients using additive manufacturing, Int. J. Pharm. 527 (2017) 21–30, https://doi.org/10.1016/j.ijpharm.2017.05.021.
[5] A. Goyanes, P. Robles Martinez, A. Buanz, A.W. Basit, S. Gaisford, Effect of geometry on drug release from 3D printed tablets, Int. J. Pharm. 494 (2015) 657–663, https://doi.org/10.1016/j.ijpharm.2015.04.069.
[6] L. Russi, C. Del Gaudio, 3D printed multicompartmental capsules for a progressive drug release, Ann. 3D Print. Med. 3 (2021), 100026, https://doi.org/10.1016/j.stlm.2021.100026.
[7] I. Seoane-Viaño, N. Gómez-Lado, H. Lázare-Iglesias, X. García-Otero, J. R. Antúnez-López, Á. Ruibal, J.J. Varela-Correa, P. Aguiar, A.W. Basit, F.J. Otero-Espinar, M. González-Barcia, A. Goyanes, A. Luzardo-Álvarez, A. Fernández-Ferreiro, 3D printed tacrolimus rectal formulations ameliorate colitis in an experimental animal model of inflammatory bowel disease, Biomedicines. 8 (2020) 563, https://doi.org/10.3390/biomedicines8120563.
[8] M. Alizadehgiashi, C.R. Nemr, M. Chekini, D. Pinto Ramos, N. Mittal, S. U. Ahmed, N. Khuu, S.O. Kelley, E. Kumacheva, Multifunctional 3D-printed wound dressings, ACS Nano 15 (2021) 12375–12387, https://doi.org/10.1021/acsnano.1c04499.
[9] Q.K. Anjani, E. Utomo, J. Domínguez-Robles, U. Detamornrat, R.F. Donnelly, E. Larrañeta, A new and sensitive HPLC-UV method for rapid and simultaneous quantification of curcumin and D-Panthenol: application to in vitro release studies of wound dressings, Molecules. 27 (2022) 1759, https://doi.org/10.3390/molecules27061759.

[10] C. Culmone, K. Lussenburg, J. Alkemade, G. Smit, A. Sakes, P. Breedveld, A fully 3D-printed steerable instrument for minimally invasive surgery, Materials (Basel) 14 (2021) 7910, https://doi.org/10.3390/ma14247910.
[11] S. Zaidi, P. Naik, S. Ahmed, Three-dimensional printed instruments used in a septoplasty: a new paradigm in surgery, Laryngoscope Investig. Otolaryngol. 6 (2021) 613–618, https://doi.org/10.1002/LIO2.579.
[12] S.A. Stewart, J. Domínguez-Robles, E. Utomo, C.J. Picco, F. Corduas, E. Mancuso, M.N. Amir, M.A. Bahar, S. Sumarheni, R.F. Donnelly, A.D. Permana, E. Larrañeta, Poly(caprolactone)-based subcutaneous implant for sustained delivery of levothyroxine, Int. J. Pharm. 607 (2021), 121011, https://doi.org/10.1016/j.ijpharm.2021.121011.
[13] S.A. Stewart, J. Domínguez-Robles, V.J. McIlorum, E. Mancuso, D.A. Lamprou, R. F. Donnelly, E. Larrañeta, Development of a biodegradable subcutaneous implant for prolonged drug delivery using 3D printing, Pharmaceutics. 12 (2020), https://doi.org/10.3390/pharmaceutics12020105.
[14] C.J. Picco, J. Domínguez-Robles, E. Utomo, A.J. Paredes, F. Volpe-Zanutto, D. Malinova, R.F. Donnelly, E. Larrañeta, 3D-printed implantable devices with biodegradable rate-controlling membrane for sustained delivery of hydrophobic drugs, Drug Deliv. 29 (2022) 1038–1048, https://doi.org/10.1080/10717544.2022.2057620.
[15] K. Vithani, A. Goyanes, V. Jannin, A.W. Basit, S. Gaisford, B.J. Boyd, An overview of 3D printing technologies for soft materials and potential opportunities for lipid-based drug delivery systems, Pharm. Res. 36 (2019) 4, https://doi.org/10.1007/s11095-018-2531-1.
[16] I. Seoane-Viaño, P. Januskaite, C. Alvarez-Lorenzo, A.W. Basit, A. Goyanes, Semi-solid extrusion 3D printing in drug delivery and biomedicine: personalised solutions for healthcare challenges, J. Control. Release 332 (2021) 367–389, https://doi.org/10.1016/j.jconrel.2021.02.027.
[17] A. Paterlini, S. Le Grill, F. Brouillet, C. Combes, D. Grossin, G. Bertrand, Robocasting of self-setting bioceramics: from paste formulation to 3D part characteristics, Open Ceram. 5 (2021), 100070, https://doi.org/10.1016/j.oceram.2021.100070.
[18] J. Domínguez-Robles, E. Utomo, V.A. Cornelius, Q.K. Anjani, A. Korelidou, Z. Gonzalez, R.F. Donnelly, A. Margariti, M. Delgado-Aguilar, Q. Tarrés, E. Larrañeta, TPU-based antiplatelet cardiovascular prostheses prepared using fused deposition modelling, Mater. Des. 220 (2022), 110837, https://doi.org/10.1016/j.matdes.2022.110837.
[19] N.K. Martin, J. Domínguez-Robles, S.A. Stewart, V.A. Cornelius, Q.K. Anjani, E. Utomo, I. García-Romero, R.F. Donnelly, A. Margariti, D.A. Lamprou, E. Larrañeta, Fused deposition modelling for the development of drug loaded cardiovascular prosthesis, Int. J. Pharm. 595 (2021), https://doi.org/10.1016/j.ijpharm.2021.120243.
[20] J. Domínguez-Robles, T. Shen, V.A. Cornelius, F. Corduas, E. Mancuso, R. F. Donnelly, A. Margariti, D.A. Lamprou, E. Larrañeta, Development of drug loaded cardiovascular prosthesis for thrombosis prevention using 3D printing, Mater. Sci. Eng. C 129 (2021), 112375, https://doi.org/10.1016/j.msec.2021.112375.
[21] J. Domínguez-Robles, L. Diaz-Gomez, E. Utomo, T. Shen, C.J. Picco, C. Alvarez-Lorenzo, A. Concheiro, R.F. Donnelly, E. Larrañeta, Use of 3D printing for the development of biodegradable antiplatelet materials for cardiovascular applications, Pharmaceuticals. 14 (2021) 921, https://doi.org/10.3390/ph14090921.
[22] R.S. de Oliveira, S.S. Fantaus, A.J. Guillot, A. Melero, R.C.R. Beck, 3D-printed products for topical skin applications: from personalized dressings to drug delivery, Pharmaceutics. 13 (2021) 1946, https://doi.org/10.3390/pharmaceutics13111946.
[23] P. Ravipati, B. Conti, E. Chiesa, K. Andrieux, Dermatillomania: strategies for developing protective biomaterials/cloth, Pharmaceutics. 13 (2021) 341, https://doi.org/10.3390/pharmaceutics13030341.
[24] Z. Muwaffak, A. Goyanes, V. Clark, A.W. Basit, S.T. Hilton, S. Gaisford, Patient-specific 3D scanned and 3D printed antimicrobial polycaprolactone wound dressings, Int. J. Pharm. 527 (2017) 161–170, https://doi.org/10.1016/j.ijpharm.2017.04.077.
[25] S. Dhall, D. Do, M. Garcia, D.S. Wijesinghe, A. Brandon, J. Kim, A. Sanchez, J. Lyubovitsky, S. Gallagher, E.A. Nothnagel, C.E. Chalfant, R.P. Patel, N. Schiller, M. Martins-Green, A novel model of chronic wounds: importance of redox imbalance and biofilm-forming bacteria for establishment of chronicity, PLoS One 9 (2014), e109848, https://doi.org/10.1371/journal.pone.0109848 [doi].
[26] S. Dhall, D.C. Do, M. Garcia, J. Kim, S.H. Mirebrahim, J. Lyubovitsky, S. Lonardi, E.A. Nothnagel, N. Schiller, M. Martins-Green, Generating and reversing chronic wounds in diabetic mice by manipulating wound redox parameters, J. Diabetes Res. 2014 (2014), 562625, https://doi.org/10.1155/2014/562625 [doi].
[27] A. Adamczak, M. Ożarowski, T.M. Karpiński, Curcumin, a natural antimicrobial agent with strain-specific activity, Pharmaceuticals. 13 (2020) 153, https://doi.org/10.3390/ph13070153.
[28] R. Mohammadinejad, H. Maleki, E. Larrañeta, A.R. Fajardo, A.B. Nik, A. Shavandi, A. Sheikhi, M. Ghorbanpour, M. Farokhi, P. Govindh, E. Cabane, S. Azizi, A.R. Aref, M. Mozafari, M. Mehrali, S. Thomas, J.F. Mano, Y.K. Mishra, V. K. Thakur, Status and future scope of plant-based green hydrogels in biomedical engineering, Appl. Mater. Today 16 (2019) 213–246, https://doi.org/10.1016/j.apmt.2019.04.010.
[29] D. Kai, M.J. Tan, P.L. Chee, Y.K. Chua, Y.L. Yap, X.J. Loh, Towards lignin-based functional materials in a sustainable world, Green Chem. 18 (2016) 1175–1200, https://doi.org/10.1039/C5GC02616D.
[30] J. Domínguez-Robles, R. Sánchez, E. Espinosa, D. Savy, P. Mazzei, A. Piccolo, A. Rodríguez, Isolation and characterization of Gramineae and Fabaceae soda lignins, Int. J. Mol. Sci. 18 (2017), https://doi.org/10.3390/ijms18020327.
[31] J. Domínguez-Robles, N.K. Martin, M.L. Fong, S.A. Stewart, N.J. Irwin, M.I. Rial-Hermida, R.F. Donnelly, E. Larrañeta, Antioxidant pla composites containing lignin for 3D printing applications: a potential material for healthcare applications, Pharmaceutics. 11 (2019), https://doi.org/10.3390/pharmaceutics11040165.
[32] E. Larrañeta, M. Imízcoz, J.X. Toh, N.J. Irwin, A. Ripolin, A. Perminova, J. Domínguez-Robles, A. Rodríguez, R.F. Donnelly, Synthesis and characterization of lignin hydrogels for potential applications as drug eluting antimicrobial coatings for medical materials, ACS Sustain. Chem. Eng. 6 (2018), https://doi.org/10.1021/acssuschemeng.8b01371.
[33] V.K. Thakur, M.K. Thakur, Recent advances in green hydrogels from lignin: a review, Int. J. Biol. Macromol. 72 (2015) 834–847, https://doi.org/10.1016/j.ijbiomac.2014.09.044.
[34] D. Liu, Y. Li, Y. Qian, Y. Xiao, S. Du, X. Qiu, Synergistic antioxidant performance of lignin and quercetin mixtures, ACS Sustain. Chem. Eng. 5 (2017) 8424–8428, https://doi.org/10.1021/acssuschemeng.7b02282.
[35] J. Domínguez-Robles, E. Larrañeta, M.L. Fong, N.K. Martin, N.J. Irwin, P. Mutjé, Q. Tarrés, M. Delgado-Aguilar, Lignin/poly(butylene succinate) composites with antioxidant and antibacterial properties for potential biomedical applications, Int. J. Biol. Macromol. 145 (2020), https://doi.org/10.1016/j.ijbiomac.2019.12.146.
[36] J. Domínguez-Robles, T. Tamminen, T. Liitiä, M.S. Peresin, A. Rodríguez, A.-S. Jääskeläinen, Aqueous acetone fractionation of kraft, organosolv and soda lignins, Int. J. Biol. Macromol. 106 (2018), https://doi.org/10.1016/j.ijbiomac.2017.08.102.
[37] J. Moohan, S.A. Stewart, E. Espinosa, A. Rosal, A. Rodríguez, E. Larrañeta, R. F. Donnelly, J. Domínguez-Robles, Cellulose nanofibers and other biopolymers for biomedical applications. A review, Appl. Sci. 10 (2020), https://doi.org/10.3390/app10010065.
[38] J. Domínguez-Robles, Q. Tarrés, M. Delgado-Aguilar, A. Rodríguez, F.X. Espinach, P. Mutjé, Approaching a new generation of fiberboards taking advantage of self lignin as green adhesive, Int. J. Biol. Macromol. 108 (2018), https://doi.org/10.1016/j.ijbiomac.2017.11.005.
[39] J. Domínguez-Robles, M.V. Palenzuela, R. Sánchez, J.M. Loaiza, E. Espinosa, A. Rosal, A. Rodríguez, Coagulation–Flocculation as an Alternative Way to Reduce the Toxicity of the Black Liquor from the Paper Industry: Thermal Valorization of the Solid Biomass Recovered, Waste and Biomass Valorization, 2019, https://doi.org/10.1007/s12649-019-00795-7.
[40] J. Domínguez-Robles, M.S. Peresin, T. Tamminen, A. Rodríguez, E. Larrañeta, A.-S. Jääskeläinen, Lignin-based hydrogels with "super-swelling" capacities for dye removal, Int. J. Biol. Macromol. 115 (2018), https://doi.org/10.1016/j.ijbiomac.2018.04.044.
[41] J. Domínguez-Robles, S.A. Stewart, A. Rendl, Z. González, R.F. Donnelly, E. Larrañeta, Lignin and cellulose blends as pharmaceutical excipient for tablet manufacturing via direct compression, Biomolecules. 9 (2019), https://doi.org/10.3390/biom9090423.
[42] P. Figueiredo, K. Lintinen, A. Kiriazis, V. Hynninen, Z. Liu, T. Bauleth-Ramos, A. Rahikkala, A. Correia, T. Kohout, B. Sarmento, J. Yli-Kauhaluoma, J. Hirvonen, O. Ikkala, M.A. Kostiainen, H.A. Santos, In vitro evaluation of biodegradable lignin-based nanoparticles for drug delivery and enhanced antiproliferation effect in cancer cells, Biomaterials. 121 (2017) 97–108.
[43] J. Domínguez-Robles, Á. Cárcamo-Martínez, S.A. Stewart, R.F. Donnelly, E. Larrañeta, M. Borrega, Lignin for pharmaceutical and biomedical applications – could this become a reality? Sustain. Chem. Pharm. 18 (2020), 100320 https://doi.org/10.1016/j.scp.2020.100320.
[44] D. Akbik, M. Ghadiri, W. Chrzanowski, R. Rohanizadeh, Curcumin as a wound healing agent, Life Sci. 116 (2014) 1–7, https://doi.org/10.1016/j.lfs.2014.08.016.
[45] C. Mohanty, M. Das, S.K. Sahoo, Sustained wound healing activity of curcumin loaded oleic acid based polymeric bandage in a rat model, Mol. Pharm. 9 (2012) 2801–2811, https://doi.org/10.1021/mp300075u.
[46] E. Proksch, R. de Bony, S. Trapp, S. Boudon, Topical use of dexpanthenol: a 70th anniversary article, J. Dermatolog. Treat. 28 (2017) 766–773, https://doi.org/10.1080/09546634.2017.1325310.
[47] R. Heise, C. Skazik, Y. Marquardt, K. Czaja, K. Sebastian, P. Kurschat, L. Gan, B. Denecke, S. Ekanayake-Bohlig, K.-P. Wilhelm, H.F. Merk, J.M. Baron, Dexpanthenol modulates gene expression in skin wound healing in vivo, Skin Pharmacol. Physiol. 25 (2012) 241–248, https://doi.org/10.1159/000341144.
[48] E. Proksch, H. Nissen, Dexapanthenol enhances skin barrier repair and reduces inflammation after sodium lauryl sulphate-induced irritation, J. Dermatolog. Treat. 13 (2002) 173–178, https://doi.org/10.1080/09546630212345674.
[49] Q.K. Anjani, J. Domínguez-Robles, E. Utomo, M. Font, M.C. Martínez-Ohárriz, A. D. Permana, Á. Cárcamo-Martínez, E. Larrañeta, R.F. Donnelly, Inclusion complexes of rifampicin with native and derivatized cyclodextrins: in silico modeling, formulation, and characterization, Pharmaceuticals 15 (2021) 20, https://doi.org/10.3390/ph15010020.
[50] T. Ak, İ. Gülçin, Antioxidant and radical scavenging properties of curcumin, Chem. Biol. Interact. 174 (2008) 27–37, https://doi.org/10.1016/j.cbi.2008.05.003.
[51] C.P. McCoy, N.J. Irwin, C. Brady, D.S. Jones, L. Carson, G.P. Andrews, S. P. Gorman, An infection-responsive approach to reduce bacterial adhesion in urinary biomaterials, Mol. Pharm. 13 (2016) 2817–2822, https://doi.org/10.1021/acs.molpharmaceut.6b00402.

[52] J.G. Hardy, E. Larrañeta, R.F. Donnelly, N. McGoldrick, K. Migalska, M.T. C. McCrudden, N.J. Irwin, L. Donnelly, C.P. McCoy, Hydrogel-forming microneedle arrays made from light-responsive materials for on-demand transdermal drug delivery, Mol. Pharm. 13 (2016) 907–914, https://doi.org/10.1021/acs.molpharmaceut.5b00807.

[53] D.S. Jones, J.G. McGovern, A.D. Woolfson, S.P. Gorman, Role of physiological conditions in the oropharynx on the adherence of respiratory bacterial isolates to endotracheal tube poly(vinyl chloride), Biomaterials. 18 (1997) 503–510, https://doi.org/10.1016/S0142-9612(96)00170-6.

[54] A.A. Miles, S.S. Misra, J.O. Irwin, The estimation of the bactericidal power of the blood, J. Hyg. 38 (1938) 732–749.

[55] K. Bonilla-Carvajal, A. Ángel-Martín, N. Moreno-Castellanos, Hipertrofia y resistencia a la insulina en un modelo in vitro de obesidad y DMT2 inducida por alta glucosa e insulina, Salud UIS 54 (2022), https://doi.org/10.18273/saluduis.54.e:22012.

[56] N.R. Moreno Castellanos, A. Angel Martin, G. Mantilla Mora, Efectos de los ácidos grasos oleico (18 : 1n-9) y palmítico (16 : 0) en el estado metabólico del adipocito, Salud UIS 53 (2021), https://doi.org/10.18273/saluduis.53.e:21009.

[57] Y. Sánchez-Cardona, C.E. Echeverri-Cuartas, M.E.L. López, N. Moreno-Castellanos, Chitosan/gelatin/PVA scaffolds for beta pancreatic cell culture, Polymers (Basel) 13 (2021) 2372, https://doi.org/10.3390/polym13142372.

[58] Y. Li, Q. Leng, X. Pang, H. Shi, Y. Liu, S. Xiao, L. Zhao, P. Zhou, S. Fu, Therapeutic effects of EGF-modified curcumin/chitosan nano-spray on wound healing, Regen. Biomater. 8 (2021), https://doi.org/10.1093/rb/rbab009.

[59] M. Ovais, I. Ahmad, A.T. Khalil, S. Mukherjee, R. Javed, M. Ayaz, A. Raza, Z. K. Shinwari, Wound healing applications of biogenic colloidal silver and gold nanoparticles: recent trends and future prospects, Appl. Microbiol. Biotechnol. 102 (2018) 4305–4318, https://doi.org/10.1007/s00253-018-8939-z.

[60] N. Moreno-Castellanos, A. Rodríguez, Y. Rabanal-Ruiz, A. Fernández-Vega, J. López-Miranda, R. Vázquez-Martínez, G. Frühbeck, M.M. Malagón, The cytoskeletal protein septin 11 is associated with human obesity and is involved in adipocyte lipid storage and metabolism, Diabetologia. 60 (2017) 324–335, https://doi.org/10.1007/s00125-016-4155-5.

[61] P. Gal, R. Kilik, M. Mokry, B. Vidinsky, T. Vasilenko, S. Mozes, N. Bobrov, Z. Tomori, J. Bober, L. Lenhardt, Simple method of open skin wound healing model in corticosteroid-treated and diabetic rats: standardization of semi-quantitative and quantitative histological assessments, Vet. Med. (Praha) 53 (2008) 652–659, https://doi.org/10.17221/1973-VETMED.

[62] B. Vidinský, P. Gál, T. Toporcer, F. Longauer, Ľ. Lenhardt, N. Bobrov, J. Sabo, Histological study of the first seven days of skin wound healing in rats, Acta Vet. Brno 75 (2006) 197–202, https://doi.org/10.2754/avb200675020197.

[63] J. Avossa, G. Herwig, C. Toncelli, F. Itel, R.M. Rossi, Electrospinning based on benign solvents: current definitions, implications and strategies, Green Chem. 24 (2022) 2347–2375, https://doi.org/10.1039/D1GC04252A.

[64] T.V. Lourencon, L.G. Greca, D. Tarasov, M. Borrega, T. Tamminen, O.J. Rojas, M. Y. Balakshin, Lignin-first integrated hydrothermal treatment (HTT) and synthesis of low-cost biorefinery particles, ACS Sustain. Chem. Eng. 8 (2020) 1230–1239, https://doi.org/10.1021/acssuschemeng.9b06511.

[65] J. Gorski, E. Proksch, J.M. Baron, D. Schmid, L. Zhang, Dexpanthenol in wound healing after medical and cosmetic interventions (postprocedure wound healing), Pharmaceuticals. 13 (2020) 138, https://doi.org/10.3390/ph13070138.

[66] W. Gehring, M. Gloor, Effect of topically applied dexpanthenol on epidermal barrier function and stratum corneum hydration, Arzneimittelforschung. 50 (2011) 659–663, https://doi.org/10.1055/s-0031-1300268.

[67] H. Stettler, P. Kurka, C. Wagner, K. Sznurkowska, O. Czernicka, A. Böhling, S. Bielfeldt, K.-P. Wilhelm, H. Lenz, A new topical panthenol-containing emollient: skin-moisturizing effect following single and prolonged usage in healthy adults, and tolerability in healthy infants, J. Dermatolog. Treat. 28 (2017) 251–257, https://doi.org/10.1080/09546634.2016.1218417.

[68] N.Z. Nagy, Z. Varga, J. Mihaly, G. Kasza, B. Ivan, E. Kiss, Highly efficient encapsulation of curcumin into and pH-controlled drug release from poly (ε-caprolactone) nanoparticles stabilized with a novel amphiphilic hyperbranched polyglycerol, Express Polym Lett 14 (2020) 90–101, https://doi.org/10.3144/expresspolymlett.2020.8.

[69] S.C. Gupta, S. Prasad, J.H. Kim, S. Patchva, L.J. Webb, I.K. Priyadarsini, B. B. Aggarwal, Multitargeting by curcumin as revealed by molecular interaction studies, Nat. Prod. Rep. 28 (2011) 1937, https://doi.org/10.1039/c1np00051a.

[70] G. Shi, Q. Cai, C. Wang, N. Lu, S. Wang, J. Bei, Fabrication and biocompatibility of cell scaffolds of poly(L-lactic acid) and poly(L-lactic-co-glycolic acid), Polym. Adv. Technol. 13 (2002) 227–232, https://doi.org/10.1002/pat.178.

[71] H. Yu, Y. Jia, C. Yao, Y. Lu, PCL/PEG core/sheath fibers with controlled drug release rate fabricated on the basis of a novel combined technique, Int. J. Pharm. 469 (2014) 17–22, https://doi.org/10.1016/j.ijpharm.2014.04.045.

[72] J. Domínguez-Robles, R. Sánchez, P. Díaz-Carrasco, E. Espinosa, M.T. García-Domínguez, A. Rodríguez, Isolation and characterization of lignins from wheat straw: application as binder in lithium batteries, Int. J. Biol. Macromol. 104 (2017), https://doi.org/10.1016/j.ijbiomac.2017.07.015.

[73] M.M. Yallapu, M. Jaggi, S.C. Chauhan, β-Cyclodextrin-curcumin self-assembly enhances curcumin delivery in prostate cancer cells, Colloids Surf. B: Biointerfaces 79 (2010) 113–125, https://doi.org/10.1016/j.colsurfb.2010.03.039.

[74] X. Chen, L.-Q. Zou, J. Niu, W. Liu, S.-F. Peng, C.-M. Liu, The stability, sustained release and cellular antioxidant activity of curcumin nanoliposomes, Molecules. 20 (2015) 14293–14311, https://doi.org/10.3390/molecules200814293.

[75] A.I. Visan, G. Popescu-Pelin, O. Gherasim, A. Mihailescu, M. Socol, I. Zgura, M. Chiritoiu, L. Elena Sima, F. Antohe, L. Ivan, D.M. Vranceanu, C.M. Cotruț, R. Cristescu, G. Socol, Long-term evaluation of dip-coated PCL-blend-PEG coatings in simulated conditions, Polymers (Basel) 12 (2020) 717, https://doi.org/10.3390/polym12030717.

[76] S.A. Stewart, J. Domínguez-Robles, V.J. McIlorum, Z. Gonzalez, E. Utomo, E. Mancuso, D.A. Lamprou, R.F. Donnelly, E. Larrañeta, Poly(caprolactone)-based coatings on 3D-printed biodegradable implants: a novel strategy to prolong delivery of hydrophilic drugs, Mol. Pharm. 17 (2020) 3487–3500, https://doi.org/10.1021/acs.molpharmaceut.0c00515.

[77] J. Domínguez-Robles, E. Espinosa, D. Savy, A. Rosal, A. Rodríguez, Biorefinery process combining Specel® process and selective lignin precipitation using mineral acids, BioResources. 11 (2016), https://doi.org/10.15376/biores.11.3.7061-7077.

[78] I.M. Comino-Sanz, M.D. López-Franco, B. Castro, P.L. Pancorbo-Hidalgo, Antioxidant dressing therapy versus standard wound care in chronic wounds (the REOX study): study protocol for a randomized controlled trial, Trials. 21 (2020) 505, https://doi.org/10.1186/s13063-020-04445-5.

[79] D. Lin, L. Xiao, W. Qin, D.A. Loy, Z. Wu, H. Chen, Q. Zhang, Preparation, characterization and antioxidant properties of curcumin encapsulated chitosan/lignosulfonate micelles, Carbohydr. Polym. 281 (2022), 119080, https://doi.org/10.1016/j.carbpol.2021.119080.

[80] S. Hewlings, D. Kalman, Curcumin: a review of its effects on human health, Foods. 6 (2017) 92, https://doi.org/10.3390/foods6100092.

[81] A. Tagami, C. Gioia, M. Lauberts, T. Budnyak, R. Moriana, M.E. Lindström, O. Sevastyanova, Solvent fractionation of softwood and hardwood kraft lignins for more efficient uses: compositional, structural, thermal, antioxidant and adsorption properties, Ind. Crop. Prod. 129 (2019) 123–134, https://doi.org/10.1016/j.indcrop.2018.11.067.

[82] I.M. Comino-Sanz, M.D. López-Franco, B. Castro, P.L. Pancorbo-Hidalgo, The role of antioxidants on wound healing: a review of the current evidence, J. Clin. Med. 10 (2021) 3558, https://doi.org/10.3390/jcm10163558.

[83] S. Roy, J.-W. Rhim, Curcumin incorporated poly(butylene adipate-co-terephthalate) film with improved water vapor barrier and antioxidant properties, Materials (Basel) 13 (2020) 4369, https://doi.org/10.3390/ma13194369.

[84] J. Zia, U.C. Paul, J.A. Heredia-Guerrero, A. Athanassiou, D. Fragouli, Low-density polyethylene/curcumin melt extruded composites with enhanced water vapor barrier and antioxidant properties for active food packaging, Polymer (Guildf) 175 (2019) 137–145, https://doi.org/10.1016/j.polymer.2019.05.012.

[85] A. Paduraru, C. Ghitulica, R. Trusca, V.A. Surdu, I.A. Neacsu, A.M. Holban, A. C. Birca, F. Iordache, B.S. Vasile, Antimicrobial wound dressings as potential materials for skin tissue regeneration, Materials (Basel) 12 (2019) 1859, https://doi.org/10.3390/ma12111859.

[86] E. Marini, M. Di Giulio, G. Magi, S. Di Lodovico, M.E. Cimarelli, A. Brenciani, A. Nostro, L. Cellini, B. Facinelli, Curcumin, an antibiotic resistance breaker against a multiresistant clinical isolate of mycobacterium abscessus, Phyther. Res. 32 (2018) 488–495, https://doi.org/10.1002/ptr.5994.

[87] Aachmann Matica, Sletta Tøndervik, Ostafe, Chitosan as a wound dressing starting material: antimicrobial properties and mode of action, Int. J. Mol. Sci. 20 (2019) 5889, https://doi.org/10.3390/ijms20235889.

[88] F.D. Lowy, Staphylococcus aureus infections, N. Engl. J. Med. 339 (1998) 520–532, https://doi.org/10.1056/NEJM199808203390806.

[89] Y. Zheng, L. He, T.K. Asiamah, M. Otto, Colonization of medical devices by staphylococci, Environ. Microbiol. 20 (2018) 3141–3153, https://doi.org/10.1111/1462-2920.14129.

[90] K.R. Aadil, S.I. Mussatto, H. Jha, Synthesis and characterization of silver nanoparticles loaded poly(vinyl alcohol)-lignin electrospun nanofibers and their antimicrobial activity, Int. J. Biol. Macromol. 120 (2018) 763–767, https://doi.org/10.1016/j.ijbiomac.2018.08.109.

[91] X. Dong, M. Dong, Y. Lu, A. Turley, T. Jin, C. Wu, Antimicrobial and antioxidant activities of lignin from residue of corn stover to ethanol production, Ind. Crop. Prod. 34 (2011) 1629–1634, https://doi.org/10.1016/j.indcrop.2011.06.002.

[92] X. Zhang, Y. Li, M. Guo, T.Z. Jin, S.A. Arabi, Q. He, B.B. Ismail, Y. Hu, D. Liu, Antimicrobial and UV blocking properties of composite chitosan films with curcumin grafted cellulose nanofiber, Food Hydrocoll. 112 (2021), 106337, https://doi.org/10.1016/j.foodhyd.2020.106337.

[93] L. Chen, Z. Song, X. Zhi, B. Du, Photoinduced antimicrobial activity of curcumin-containing coatings: molecular interaction, stability and potential application in food decontamination, ACS Omega 5 (2020) 31044–31054, https://doi.org/10.1021/acsomega.0c04065.

[94] Y. Liu, Y. Cai, X. Jiang, J. Wu, X. Le, Molecular interactions, characterization and antimicrobial activity of curcumin–chitosan blend films, Food Hydrocoll. 52 (2016) 564–572, https://doi.org/10.1016/j.foodhyd.2015.08.005.

[95] S. Kaur, N.H. Modi, D. Panda, N. Roy, Probing the binding site of curcumin in Escherichia coli and Bacillus subtilis FtsZ – a structural insight to unveil antibacterial activity of curcumin, Eur. J. Med. Chem. 45 (2010) 4209–4214, https://doi.org/10.1016/j.ejmech.2010.06.015.

[96] T.J. Kinnari, J. Esteban, N.Z. Martin-de-Hijas, O. Sánchez-Muñoz, S. Sánchez-Salcedo, M. Colilla, M. Vallet-Regí, E. Gomez-Barrena, Influence of surface porosity and pH on bacterial adherence to hydroxyapatite and biphasic calcium phosphate bioceramics, J. Med. Microbiol. 58 (2009) 132–137, https://doi.org/10.1099/jmm.0.002758-0.

[97] T.J. Kinnari, J. Esteban, E. Gomez-Barrena, N. Zamora, R. Fernandez-Roblas, A. Nieto, J.C. Doadrio, A. López-Noriega, E. Ruiz-Hernández, D. Arcos, M. Vallet-Regí, Bacterial adherence to SiO2-based multifunctional bioceramics, J. Biomed. Mater. Res. Part A (2008), https://doi.org/10.1002/jbm.a.31943.

[98] P. Ghasemiyeh, S. Mohammadi-Samani, Polymers blending as release modulating tool in drug delivery, Front. Mater. 8 (2021), https://doi.org/10.3389/fmats.2021.752813.
[99] J. Zeng, X. Xu, X. Chen, Q. Liang, X. Bian, L. Yang, X. Jing, Biodegradable electrospun fibers for drug delivery, J. Control. Release 92 (2003) 227–231, https://doi.org/10.1016/S0168-3659(03)00372-9.
[100] J. Domínguez-Robles, C. Mancinelli, E. Mancuso, I. García-Romero, B.F. Gilmore, L. Casettari, E. Larrañeta, D.A. Lamprou, 3D printing of drug-loaded thermoplastic polyurethane meshes: a potential material for soft tissue reinforcement in vaginal surgery, Pharmaceutics. 12 (2020), https://doi.org/10.3390/pharmaceutics12010063.
[101] T. Zehnder, T. Freund, M. Demir, R. Detsch, A. Boccaccini, Fabrication of cell-loaded two-phase 3D constructs for tissue engineering, Materials (Basel) 9 (2016) 887, https://doi.org/10.3390/ma9110887.
[102] E. Utomo, J. Domínguez-Robles, N. Moreno-Castellanos, S.A. Stewart, C.J. Picco, Q.K. Anjani, J.A. Simón, I. Peñuelas, R.F. Donnelly, E. Larrañeta, Development of intranasal implantable devices for schizophrenia treatment, Int. J. Pharm. 624 (2022), 122061, https://doi.org/10.1016/j.ijpharm.2022.122061.
[103] R.-Y. Li, Z.-G. Liu, H.-Q. Liu, L. Chen, J.-F. Liu, Y.-H. Pan, Evaluation of biocompatibility and toxicity of biodegradable poly (DL-lactic acid) films, Am. J. Transl. Res. 7 (2015) 1357–1370.
[104] B. Dhandayuthapani, Y. Yoshida, T. Maekawa, D.S. Kumar, Polymeric scaffolds in tissue engineering application: a review, Int. J. Polym. Sci. 2011 (2011) 1–19, https://doi.org/10.1155/2011/290602.
[105] C.X.F. Lam, M.M. Savalani, S.-H. Teoh, D.W. Hutmacher, Dynamics of in vitro polymer degradation of polycaprolactone-based scaffolds: accelerated versus simulated physiological conditions, Biomed. Mater. 3 (2008), 034108, https://doi.org/10.1088/1748-6041/3/3/034108.
[106] S. Devadas, S.M.N. Al-Ajrash, D.A. Klosterman, K.M. Crosson, G.S. Crosson, E. S. Vasquez, Fabrication and characterization of electrospun poly(acrylonitrile-co-methyl acrylate)/lignin nanofibers: effects of lignin type and total polymer concentration, Polymers (Basel) 13 (2021) 992, https://doi.org/10.3390/polym13070992.
[107] G. Jaganathan, K. Manivannan, S. Lakshmanan, M.A. Sithique, Fabrication and characterization of Artocarpus heterophyllus waste derived lignin added chitosan biocomposites for wound dressing application, Sustain. Chem. Pharm. 10 (2018) 27–32, https://doi.org/10.1016/j.scp.2018.08.002.
[108] N. Nan, W. Hu, J. Wang, Lignin-based porous biomaterials for medical and pharmaceutical applications, Biomedicines. 10 (2022) 747, https://doi.org/10.3390/biomedicines10040747.
[109] K. Ravishankar, M. Venkatesan, R.P. Desingh, A. Mahalingam, B. Sadhasivam, R. Subramaniyam, R. Dhamodharan, Biocompatible hydrogels of chitosan-alkali lignin for potential wound healing applications, Mater. Sci. Eng. C 102 (2019) 447–457, https://doi.org/10.1016/j.msec.2019.04.038.
[110] J. Wang, L. Tian, B. Luo, S. Ramakrishna, D. Kai, X.J. Loh, I.H. Yang, G.R. Deen, X. Mo, Engineering PCL/lignin nanofibers as an antioxidant scaffold for the growth of neuron and Schwann cell, Colloids Surf. B: Biointerfaces 169 (2018) 356–365, https://doi.org/10.1016/j.colsurfb.2018.05.021.
[111] S. Fahimirad, H. Abtahi, P. Satei, E. Ghaznavi-Rad, M. Moslehi, A. Ganji, Wound healing performance of PCL/chitosan based electrospun nanofiber electrosprayed with curcumin loaded chitosan nanoparticles, Carbohydr. Polym. 259 (2021), 117640, https://doi.org/10.1016/j.carbpol.2021.117640.
[112] V.V.S.R. Karri, G. Kuppusamy, S.V. Talluri, S.S. Mannemala, R. Kollipara, A. D. Wadhwani, S. Mulukutla, K.R.S. Raju, R. Malayandi, Curcumin loaded chitosan nanoparticles impregnated into collagen-alginate scaffolds for diabetic wound healing, Int. J. Biol. Macromol. 93 (2016) 1519–1529, https://doi.org/10.1016/j.ijbiomac.2016.05.038.
[113] M. Mobaraki, D. Bizari, M. Soltani, H. Khshmohabat, K. Raahemifar, M. Akbarzade Amirdehi, The effects of curcumin nanoparticles incorporated into collagen-alginate scaffold on wound healing of skin tissue in trauma patients, Polymers (Basel) 13 (2021) 4291, https://doi.org/10.3390/polym13244291.
[114] M. Najafiasl, S. Osfouri, R. Azin, S. Zaeri, Alginate-based electrospun core/shell nanofibers containing dexpanthenol: a good candidate for wound dressing, J. Drug Deliv. Sci. Technol. 57 (2020), 101708, https://doi.org/10.1016/j.jddst.2020.101708.
[115] K. Biro, D. ThaCi, F.R. Ochsendorf, R. Kaufmann, W.-H. Boehncke, Efficacy of dexpanthenol in skin protection against irritation: a double-blind, placebo-controlled study, Contact Dermatitis 49 (2003) 80–84, https://doi.org/10.1111/j.0105-1873.2003.00184.x.
[116] D.G. Sami, H.H. Heiba, A. Abdellatif, Wound healing models: a systematic review of animal and non-animal models, Wound Med. 24 (2019) 8–17, https://doi.org/10.1016/j.wndm.2018.12.001.
[117] A. Grada, J. Mervis, V. Falanga, Research techniques made simple: animal models of wound healing, J. Invest. Dermatol. 138 (2018) 2095–2105.e1, https://doi.org/10.1016/j.jid.2018.08.005.
[118] D.S. Masson-Meyers, T.A.M. Andrade, G.F. Caetano, F.R. Guimaraes, M.N. Leite, S.N. Leite, M.A.C. Frade, Experimental models and methods for cutaneous wound healing assessment, Int. J. Exp. Pathol. 101 (2020) 21–37, https://doi.org/10.1111/iep.12346.
[119] E. Grambow, H. Sorg, C.G.G. Sorg, D. Strüder, Experimental models to study skin wound healing with a focus on angiogenesis, Med. Sci. 9 (2021) 55, https://doi.org/10.3390/medsci9030055.
[120] F. Anjum, N.A. Agabalyan, H.D. Sparks, N.L. Rosin, M.S. Kallos, J. Biernaskie, Biocomposite nanofiber matrices to support ECM remodeling by human dermal progenitors and enhanced wound closure, Sci. Rep. 7 (2017) 1–17, https://doi.org/10.1038/s41598-017-10735-x.
[121] A. Oguz, O. Uslukaya, U. Alabalık, A. Turkoglu, M. Kapan, Z. Bozdag, Topical N-acetylcysteine improves wound healing comparable to dexpanthenol: an experimental study, Int. Surg. 100 (2015) 656–661, https://doi.org/10.9738/INTSURG-D-14-00227.1.
[122] G. Hulsart-Billström, J. Dawson, S. Hofmann, R. Müller, M. Stoddart, M. Alini, R. Redl, A. El Haj, R. Brown, V. Salih, J. Hilborn, S. Larsson, R. Oreffo, A surprisingly poor correlation between in vitro and in vivo testing of biomaterials for bone regeneration: results of a multicentre analysis, Eur. Cells Mater. 31 (2016) 312–322, https://doi.org/10.22203/eCM.v031a20.
[123] R.L. Juliano, S. Haskill, Signal transduction from the extracellular matrix, J. Cell Biol. 120 (1993) 577–585, https://doi.org/10.1083/jcb.120.3.577.
[124] H.-N. Kung, M.-J. Yang, C.-F. Chang, Y.-P. Chau, K.-S. Lu, In vitro and in vivo wound healing-promoting activities of β-lapachone, Am. J. Physiol. Physiol. 295 (2008) C931–C943, https://doi.org/10.1152/ajpcell.00266.2008.
[125] B. Rai, J.L. Lin, Z.X.H. Lim, R.E. Guldberg, D.W. Hutmacher, S.M. Cool, Differences between in vitro viability and differentiation and in vivo bone-forming efficacy of human mesenchymal stem cells cultured on PCL–TCP scaffolds, Biomaterials. 31 (2010) 7960–7970, https://doi.org/10.1016/j.biomaterials.2010.07.001.